



Benchmarking Self-Supervised Learning Methods for Accelerated MRI Reconstruction

Andrew Wang 
School of Engineering
University of Edinburgh
andrew.wang@ed.ac.uk

Steven McDonagh 
School of Engineering
University of Edinburgh

Mike Davies 
School of Engineering
University of Edinburgh

SSIBench: Self-Supervised Imaging Benchmark

andrewwango.github.io/ssibench

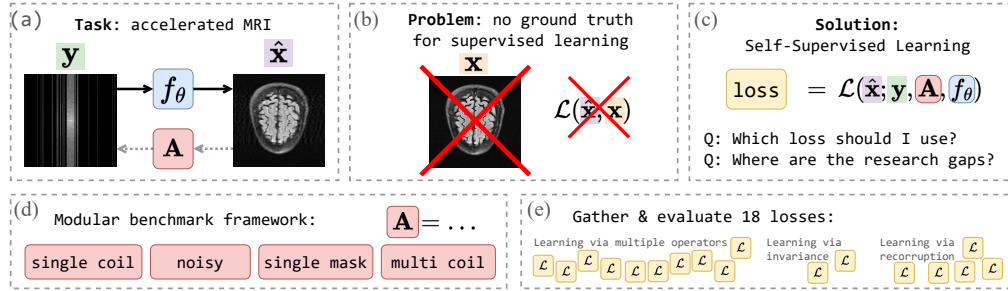


Figure 1: (a) Accelerated MRI reconstruction from undersampled images y . (b) Ground truth (GT) images x are impossible or expensive to obtain. (c) There has been a recent surge in self-supervised imaging (SSI) methods that can learn without GT. (d) We introduce **SSIBench**, a modular benchmark over multiple MRI forward operators A , that gathers and evaluates 18 state-of-the-art methods (e).

Abstract

Reconstructing MRI from highly undersampled measurements is crucial for accelerating medical imaging, but is challenging due to the ill-posedness of the inverse problem. While supervised deep learning (DL) approaches have shown remarkable success, they traditionally rely on fully-sampled ground truth (GT) images, which are expensive or impossible to obtain in real scenarios. This problem has created a recent surge in interest in self-supervised learning methods that do not require GT. Although recent methods are now fast approaching “oracle” supervised performance, the lack of systematic comparison and standard experimental setups are hindering targeted methodological research and precluding widespread trustworthy industry adoption. We present **SSIBench**, a modular and flexible comparison framework to unify and thoroughly benchmark Self-Supervised Imaging methods (SSI) without GT. We evaluate 18 methods across 4 realistic MRI scenarios on real data, showing a wide performance landscape whose method ranking differs across scenarios and metrics, exposing the need for further SSI research. Our insights also show how complementary methods could be compounded for future improvements, exemplified by a novel loss we propose, **Multi-Operator Equivariant Imaging**. To accelerate reproducible research and lower the barrier to entry, we provide the extensible benchmark and open-source reimplementations of all methods at <https://andrewwango.github.io/ssibench>, allowing researchers to rapidly and fairly contribute and evaluate new methods on the standardised setup for potential leaderboard ranking, or benchmark existing methods on custom datasets, forward operators, or models, unlocking the application of SSI to other valuable GT free domains such as 4D MRI and other nascent scientific imaging modalities.

1 Introduction

Accelerating MRI reconstruction is crucial for reducing lengthy scan times, modelled as [49]:

$$\mathbf{y}_{i,c} = \mathbf{A}_{i,c}\mathbf{x}_i + \epsilon, \quad \mathbf{A}_{i,c} = \mathbf{M}_i\mathbf{F}\mathbf{S}_c, \quad \epsilon \sim \mathcal{N}(\mathbf{0}, \sigma^2\mathbf{I}), \quad (1)$$

where $\mathbf{x}_i \in \mathcal{X} \in \mathbb{R}^n$ are the i -th underlying images, $\mathbf{y}_i = \{\mathbf{y}_{i,c}\}_{c=1}^C \in \mathcal{Y} \in \mathbb{R}^m$ are the k space measurements, $\mathbf{A}_i = \{\mathbf{A}_{i,c}\}_{c=1}^C$ is the *forward operator* (or *acquisition method*), consisting of the undersampling mask \mathbf{M}_i , the c -th coil sensitivity map \mathbf{S}_c and the Fourier operator \mathbf{F} , and $m = n/\alpha$ where α is the acceleration rate. The goal is to recover $\hat{\mathbf{x}}_i = f_\theta(\mathbf{y}_i, \mathbf{A}_i)$ via a *model* f_θ , but due to the undersampling $m < n$ the null-space is non-trivial $\mathcal{N}(\mathbf{A}) \in \mathbb{R}^{n-m}$, leading to a challenging ill-posed inverse problem where one must reconstruct high quality images from partial, noisy measurements.

Classical compressed sensing solves the problem using regularised optimisation [49]. However, this requires hand-crafted, image-specific priors, inference is lengthy and expensive, and acceleration rates may be limited [33]. Deep learning has been used to learn f_θ directly from data, and achieves impressive results compared to classical methods [33, 42, 78]. Prevailing methods assume that underlying ground-truth (GT) images \mathbf{x} are available in order to train with supervised learning $\mathcal{L}_{\text{sup}} = \ell(\hat{\mathbf{x}}, \mathbf{x})$ where $\ell(\cdot, \cdot)$ is any metric such as the mean squared error (MSE).

However, fully-sampled GT measurements are impossible or expensive to obtain in real scenarios, *e.g.* when imaging moving organs [84], 4D MRI [59], low-field MRI [39], or where it leads to blurring in the case of prolonged patient motion. Therefore, **self-supervised imaging (SSI) *i.e.* methods that learn without access to GT \mathbf{x}** are needed. Here, *self-supervised* is synonymous with *unsupervised*, and differs from the definition of SSL in representation learning. Here, images are output $\hat{\mathbf{x}} = f_\theta(\mathbf{y})$ rather than input, and GT \mathbf{x} means images rather than labels.

A vast array of SSI methods have been proposed in recent years. However, they often fail to compare to existing methods, exacerbated by disjoint communities of researchers working on the same problem, *e.g.* from ML research, imaging, or various medical or non-medical imaging application domains. It is hence difficult to draw direct comparisons due to different or proprietary setups, datasets, a vast variety of models f_θ , forward operators \mathbf{A} , evaluation protocols or lack of transparent implementation of compared methods; furthermore, each proposed method claims to perform best. This prevents research focussed on where true gaps lie, and impedes trustworthy translation of SSI into industry.

Our benchmark unifies previously fractured efforts by providing a standardised, objective evaluation of methods, leading to trustworthy application. It also provides the opportunity for ML researchers to find unsolved gaps exposed in the common framework and clear performance landscape, and collectively contribute methodological advances to solve real-world and future imaging problems. By making the benchmark modular and accessible to the public, researchers can *a)* rapidly implement new methods or combine existing ones and fairly test these on the standard setup or *b)* evaluate them on custom datasets, models f_θ , or forward operators \mathbf{A} , or as a blueprint for other challenging nascent scientific imaging problems within and beyond MRI, where lack-of-GT currently hurts progress.

We clarify the scope of our benchmark. Our benchmark investigates methods that possess the following properties. We provide further discussion and examples on method scope in Appendix A.

1. *Feedforward methods*, which are desirable because they provide fast inference by requiring only one neural function evaluation per image (NFE) $N = 1$ (or $N < 10$ in the case of unrolled networks), rather than methods that require lengthy iterative procedures at inference such as diffusion models ($N \sim 10^2$ to 4) or other examples listed in Appendix A. The latter are currently impractical in real-world clinical application.
2. *Ground-truth-free *i.e.* self-supervised methods*, which learn from only $\{\mathbf{y}_i\}$, as GT $\{\mathbf{x}_i\}$ is not available during training, nor during pretraining of generative priors.
3. *Architecture-agnostic methods* that do not depend on a specific model architecture, such that the learning is primarily guided by the loss function rather than the inductive bias of very specific architectures. This way, our findings generalise to future architectures, rather than being limited to current modality-specific architectures.

We provide extensive experimental results benchmarking these methods on accelerated MRI reconstruction without GT across four acquisition scenarios \mathbf{A} , which are justified and sufficiently general

to be applied to future problems, and provide the loss reimplementations, living benchmark and training code at <https://andrewwango.github.io/ssibench>.

1.1 Contributions

1. A comprehensive review unifying SotA self-supervised feedforward imaging methods;
2. Reproducible, well-documented and pytested reimplementations of 18 methods, and a modular benchmark site facilitating contribution and application to other problems;
3. Benchmarking experiments for accelerated MRI reconstruction without GT across four insightful scenarios on a standardised setup, where different methods have different strengths;
4. A new method, multi-operator equivariant imaging (MO-EI), made possible by simply combining two distinct methods from the benchmark, that outperforms or is competitive with all existing methods and approaches supervised learning performance.

2 SSIBench - a benchmark for self-supervised imaging

2.1 Benchmark methodology

We provide a systematic review of existing SotA feedforward self-supervised methods from the literature that fall under our scope mentioned above, and unify these by constructing **SSIBench** as follows. Similar to [53, 78], we highlight the loss function $\mathcal{L}(\hat{\mathbf{x}}; \mathbf{y}, \mathbf{A}, f_\theta)$ as the key conceptual advance that differs between methods. To provide a fair, substantive comparison and maximise compatibility of our benchmark to different setups, we evaluate the losses while fixing all other elements of the experimental setup, including the forward operator \mathbf{A} , the type, architecture and size of the model f_θ (such that all methods have the same inductive bias), data preprocessing stages, and the metrics. This decision is crucial for controlled comparisons of loss functions, so that the modular benchmark can easily be adapted with any model f_θ , forward operator \mathbf{A} or dataset of the future.

In this framework we gather 18 distinct ground-truth-free loss functions $\mathcal{L}(\hat{\mathbf{x}}; \mathbf{y}, \mathbf{A}, f_\theta)$ from across the ML and imaging literatures, summarised in Table 1. We reimplement these into the DeepInverse library¹ [77], since the compared methods’ original codebases often adhere to differing software engineering principles and are often implemented for their specific experimental setups with poor generalisability to other setups. We provide details of their generalised implementations and sketches of the code mapped to their equations in Appendix B.3. Following standard modern coding best practice, all code contributed to DeepInverse is unit-tested, code-reviewed and thoroughly documented.

2.2 Benchmark scenarios

We consider four common accelerated MRI experimental scenarios to provide insight on the performance of the methods on individual controlled tasks. This is preferable to the often reported way of experimenting on an amalgamated task *e.g.* noisy data with unknown sensitivity maps [53, 90], as it would be unclear whether differences in performance are actually due to reconstruction ability, or other MRI sub-tasks such as joint coil sensitivity map estimation.

Scenario 1 (Single-coil) Measurements are single-coil $C = 1$, noiseless $\sigma = 0$ and retrospectively undersampled to $6\times$ acceleration, with a random mask per sample $\mathbf{M}_i \sim \mathcal{M}$. This is a simplified but nonetheless very important setup where no additional information is provided by multiple coils, so we can demonstrate performance on recovering data from the clear null-space of the rank-deficient forward operator $\mathcal{N}(\mathbf{A}) \in \mathbb{R}^{n-m}$.

Scenario 2 (Noisy) Similar to scenario 1, but simulated with known $\sigma > 0$, a realistic model for MRI acquisition [54], where methods must perform joint reconstruction and denoising.

Scenario 3 (Single-operator) Similar to scenario 1, but with a fixed sampling mask $\mathbf{M}_i = \mathbf{M} \forall i$, common in clinical systems where a predetermined vendor-optimized sampling pattern is used to simplify hardware constraints and ensure consistency across patients. Here, the assumption required for methods that learn from multiple operators is not met.

¹<https://deepinv.github.io>

Table 1: Self-supervised losses gathered, reimplemented and evaluated in our benchmark framework. Above: losses for reconstruction. Below: losses for joint reconstruction and denoising.

Method	Ref	Loss	Code: <code>deepinv.loss._____</code>
MC	[70]	Eq. (2)	<code>MCloss()</code>
SSDU	[91]	Eq. (3)	<code>SplittingLoss()</code>
Noise2Inverse	[34]	Eq. (4)	<code>SplittingLoss()</code>
Weighted-SSDU	[53]	Eq. (5)	<code>WeightedSplittingLoss()</code>
SSDU-Consistency	[35]	Eq. (6)	<code>SplittingConsistencyLoss()</code>
CC-SSDU	[95]	Eq. (8)+Eq. (3)	<code>MOConsistencyLoss() + SplittingLoss()</code>
Adversarial	[17]	Eq. (12)	<code>UnsupAdversarialGeneratorLoss()</code>
UAIR	[61]	Eq. (13)	<code>UAIRGeneratorLoss()</code>
VORTEX	[22]	Eq. (11)	<code>AugmentConsistencyLoss()</code>
EI	[12]	Eq. (9)	<code>EILoss()</code>
MOI	[78]	Eq. (7)	<code>MOILoss()</code>
MO-EI	Ours	Eq. (10)	<code>MOEILoss()</code>
ENSURE	[5]	Eq. (15)	<code>ENSURELoss()</code>
DDSSL	[66]	[63]+Eq. (9)	<code>R2RLoss() + EILoss()</code>
Robust-SSDU	[54]	Eq. (16)	<code>RobustSplittingLoss()</code>
Noise2Recon-SSDU	[23]	Eq. (5)+Eq. (11)	<code>WeightedSplittingLoss()</code> <code>+ AugmentConsistencyLoss()</code>
Robust-EI	[13]	Eq. (9)+Eq. (14)	<code>EILoss() + SUREGaussianLoss()</code>
Robust-MO-EI	Ours	Eq. (10)+Eq. (14)	<code>MOEILoss() + SUREGaussianLoss()</code>

Scenario 4 (Multi-coil) Similar to scenario 1, but $C > 1$, the prevailing model for modern MRI parallel imaging acquisition [75]. Since now m is $C \times$ larger, the effective null-space is smaller; see Appendix C.2 for an analysis. We assume known sensitivity maps.

The experimental setup is described and justified in Section 3 and further details are in Appendix B.

2.3 Benchmarked methods

We formulate the 18 benchmarked losses; details on their reimplementations are in Appendix B.3.

Measurement consistency (MC) The most basic self-supervised loss [70] simply computes:

$$\mathcal{L}_{\text{MC}} = \ell(\mathbf{A}\hat{\mathbf{x}}, \mathbf{y}), \quad (2)$$

The MC loss cannot recover information from the operator’s null-space $\mathcal{N}(\mathbf{A})$ as infinitely many solutions $\mathbf{A}^\dagger \mathbf{y} + \mathbf{v}$ can satisfy $\mathcal{L}_{\text{MC}} = 0$ where $\mathbf{v} \in \mathcal{N}(\mathbf{A})$. [92] showed that MC [70] performed worse than SENSE [64]. MC also has been used in the presence of strong inductive bias where the regularisation is provided by the very specific architectures [20, 43, 80] or initialisations [21]. However, to disentangle this we focus on comparing the performance of different loss functions while using identical networks. [83, 7] add traditional regularising terms (*e.g.* sparsity) to MC: in general, such terms can always be independently appended to any of the losses considered in this paper.

Learning from measurement splitting Measurement splitting methods, including SSDU and similar works [91, 90, 3, 38, 42], randomly split \mathbf{y} into two sets at each instance during training:

$$\mathcal{L}_{\text{SSDU}} = \ell(\mathbf{M}_2 \mathbf{A} f_\theta(\mathbf{M}_1 \mathbf{y}, \mathbf{M}_1 \mathbf{A}), \mathbf{M}_2 \mathbf{y}), \quad \hat{\mathbf{x}} = f_\theta(\mathbf{y}, \mathbf{A}) \quad (3)$$

where \mathbf{M}_1 is a randomly generated mask (spanning the whole measurement domain in expectation), $\mathbf{M}_1 + \mathbf{M}_2 = \mathbb{I}_m$. [88, 36, 30, 37, 31, 46] require pairs of measurements of the same subject; these are equivalent to SSDU but with $2 \times$ less acceleration. [86] use the same concept applied to a specific sampling mask \mathbf{A} . An inference-time adaptation averages over multiple passes, inspired by [34]:

$$\hat{\mathbf{x}} = \frac{1}{N} \sum_{n=1}^N f_\theta(\mathbf{M}_n \mathbf{y}, \mathbf{M}_n \mathbf{A}). \quad (4)$$

[53] propose a weighting to the SSDU loss metric $\ell(\cdot, \cdot)$ and an informed splitting strategy $\mathbf{M}_1 \sim \mathcal{M}$, where $\mathbf{P} = \mathbb{E}[\mathbf{M}]$, $\tilde{\mathbf{P}} = \mathbb{E}[\mathbf{M}_1]$ i.e. the PDFs of the imaging mask and the splitting mask, respectively:

$$\mathcal{L}_{\text{Weighted-SSDU}} = \mathcal{L}_{\text{SSDU}}, \ell(a, b) := \|(1 - \mathbf{K})^{-\frac{1}{2}}(a - b)\|_2^2, \mathbf{K} = (\mathbb{I}_n - \tilde{\mathbf{P}}\mathbf{P})^{-1}(\mathbb{I}_n - \mathbf{P}), \quad (5)$$

[35, 97, 87] splits \mathbf{y} with both $\mathbf{M}_1, \mathbf{M}_2$, computes a SSDU-style loss for each of these subsets, and also computes a consistency loss between the two reconstructions $\hat{\mathbf{x}}_1, \hat{\mathbf{x}}_2$, where $\tilde{\mathbf{A}} = (\mathbf{I} - \mathbf{M})\mathbf{F}\mathbf{S}$:

$$\mathcal{L}_{\text{SSDU-Consistency}} = \ell(\mathbf{A}\hat{\mathbf{x}}_1, \mathbf{y}) + \ell(\mathbf{A}\hat{\mathbf{x}}_2, \mathbf{y}) + \ell(\tilde{\mathbf{A}}\hat{\mathbf{x}}_1, \tilde{\mathbf{A}}\hat{\mathbf{x}}_2), \hat{\mathbf{x}}_k = f_\theta(\mathbf{M}_k\mathbf{y}, \mathbf{M}_k\mathbf{A}), \quad (6)$$

Learning from multiple operators These approaches leverage the fact that the image training set is seen through multiple $\mathbf{A}_i \sim \mathcal{A}$, where \mathcal{A} is the operator set of same order as the mask set $|\mathcal{M}| = \binom{n}{m}$. Multi-Operator Imaging [78] leverages this by drawing a random operator $\tilde{\mathbf{A}} \sim \mathcal{A}$ at each forward pass and regularises the MC loss with another loss that encourages consistency of f_θ over \mathbf{A}_i , shown to theoretically enable the function to learn in the null-space:

$$\mathcal{L}_{\text{MOI}} = \mathcal{L}_{\text{MC}} + \ell(\hat{\mathbf{x}}, f_\theta(\tilde{\mathbf{A}}\hat{\mathbf{x}}, \tilde{\mathbf{A}})), \hat{\mathbf{x}} = f_\theta(\mathbf{y}, \mathbf{A}). \quad (7)$$

[95] constructs a very similar loss to MOI, instead enforcing consistency on the measurement \mathbf{y} :

$$\mathcal{L}_{\text{CC-SSDU}} = \mathcal{L}_{\text{SSDU}} + \ell(\mathbf{y}, \mathbf{A}f_\theta(\tilde{\mathbf{A}}\hat{\mathbf{x}}, \tilde{\mathbf{A}})). \quad (8)$$

Learning from invariance Equivariant Imaging (EI) [12, 13, 85, 84] leverages a natural assumption that \mathcal{X} is invariant to a group G of transformations $g \circ \mathbf{x} \in \mathcal{X} \forall \mathbf{x} \in \mathcal{X}, g \in G$. The image set can then be interpreted as being observed through a set of multiple transformed operators $\mathbf{A} \circ g(\cdot)$ of order $|G|$, allowing the solver to “see” into the null-space. The assumption is constrained using:

$$\mathcal{L}_{\text{EI}} = \mathcal{L}_{\text{MC}} + \ell(\mathbf{T}_g\hat{\mathbf{x}}, f_\theta(\mathbf{A}\mathbf{T}_g\hat{\mathbf{x}}, \mathbf{A})), \hat{\mathbf{x}} = f_\theta(\mathbf{y}, \mathbf{A}), \quad (9)$$

where \mathbf{T}_g is an action of G , which, for MRI images, we use 2D rotations for G following [13].

Combining two methods Our benchmark makes a new loss function apparent, which we can rapidly implement and test. Since adding more, well-targeted regularisation typically improves the stability and generalisation of the model, and that the operators leveraged by MOI (multiple physical operators) and EI (multiple virtual operators) are complementary, we propose a hybrid Multi-Operator Equivariant Imaging loss that unifies these strategies. Naturally, several other complementary combinations (e.g. SSDU + EI) remain to be explored. Assume that the image set is imaged by the *augmented operator set* $\mathcal{A}_G = \{\mathbf{A}_i\mathbf{T}_g \mid \forall \mathbf{A}_i \in \mathcal{A}, g \in G\}$, the orbit space of \mathcal{A} under G . Since $|\mathcal{A}_G| \approx |\mathcal{A}||G|$ is much larger than in MOI or EI, we expect to provide more regularisation and thereby improve the performance. We leverage the augmented operator set using the loss function:

$$\mathcal{L}_{\text{MO-EI}} = \mathcal{L}_{\text{MC}} + \ell(\mathbf{T}_g\hat{\mathbf{x}}, f_\theta(\tilde{\mathbf{A}}_g\hat{\mathbf{x}}, \tilde{\mathbf{A}}_g)), \tilde{\mathbf{A}}_g \sim \mathcal{A}_G. \quad (10)$$

For the group G , since we have soft deformable tissue [31], we expect \mathcal{X} be invariant to the group of perturbative C^1 -diffeomorphisms. See Appendix B.3 for more details.

Data augmentation EI is related to data augmentation [14], which, when GT \mathbf{x} is available, can be used to constrain invariance or equivariance on \mathbf{x} [28]. Data augmentation consistency (DAC) methods [89] such as VORTEX [22] build on this in the semi-supervised context by performing data augmentation on \mathbf{y} when GT is not available, chiefly to provide robustness to OOD data:

$$\mathcal{L}_{\text{VORTEX}} = \begin{cases} \mathcal{L}_{\text{sup}}(f_\theta(\mathbf{y}, \mathbf{A}), \mathbf{x}) & \text{if GT exists} \\ \ell(\mathbf{T}_2 f_\theta(\mathbf{y}, \mathbf{A}), f_\theta(\mathbf{T}_1 \mathbf{y}, \mathbf{A}\mathbf{T}_2^{-1})) & \text{otherwise} \end{cases} \quad (11)$$

where $\mathbf{T}_1, \mathbf{T}_2$ are random transforms in k -space (e.g. add noise, phase shift) and image space. We test the ability of DAC methods in the fully GT free case, replacing \mathcal{L}_{sup} with \mathcal{L}_{MC} to enforce MC.

Adversarial losses Adversarial losses have been proposed to reconstruct MRI via the dual training of f_θ and a discriminator D . While unconditional, generative adversarial networks [9] are not feedforward at inference time, [17] propose a feedforward method with an adversarial loss:

$$\mathcal{L}_{\text{adversarial}} = D(\tilde{\mathbf{A}}f_\theta(\mathbf{y}, \mathbf{A}), \tilde{\mathbf{y}}), \quad (12)$$

where $\tilde{\mathbf{y}} \sim \mathcal{Y}$ *i.e.* another randomly sampled “real” measurement from the training dataset \mathcal{Y} . The aim of D is to distinguish between reconstructed measurements and training measurements, such that the aim of f_θ is to reconstruct high quality measurements that are indistinguishable from “real” measurements. Note that it is unclear how [17] can learn the unknown signal model and recover information from the null-space. UAIR [61] is a related method originally proposed for inpainting, using a multi-step loss consisting of adversarial and measurement consistency terms:

$$\hat{\mathbf{y}} = \tilde{\mathbf{A}}f_\theta(\mathbf{y}, \mathbf{A}), \quad \mathcal{L}_{\text{UAIR}} = D(\hat{\mathbf{y}}, \mathbf{y}) + \ell(\tilde{\mathbf{A}}f_\theta(\hat{\mathbf{y}}, \tilde{\mathbf{A}}), \hat{\mathbf{y}}). \quad (13)$$

Joint reconstruction and denoising We consider composite losses used for jointly learning to reconstruct and denoise from partial noisy measurements $\sigma > 0$ alone. Several self-supervised denoising losses exist in the literature [79]; most combinations of these with reconstruction losses are yet to be explored. Stein’s Unbiased Risk Estimator (SURE) [76, 67] can be used in place of \mathcal{L}_{MC} and is shown in [13] to be an unbiased estimator of \mathcal{L}_{MC} . It can be seen as further “reoccurring” data:

$$\mathcal{L}_{\text{SURE}} = \mathcal{L}_{\text{MC}} + \frac{2\sigma^2}{\tau} \mathbf{b}^\top (\mathbf{A}f_\theta(\mathbf{y} + \tau\mathbf{b}, \mathbf{A}) - \mathbf{A}f_\theta(\mathbf{y}, \mathbf{A})) - \sigma^2, \quad (14)$$

where $\mathbf{b} \sim \mathcal{N}(\mathbf{0}, \mathbf{I})$, τ is a hyperparameter and $\mathbb{E}_{\mathbf{y}}[\mathcal{L}_{\text{SURE}}] = \mathbb{E}_{\mathbf{x}, \mathbf{y}}[\ell(\mathbf{A}f_\theta(\mathbf{y}), \mathbf{Ax})]$. Robust-EI [13] then simply use $\mathcal{L}_{\text{Robust-EI}} = \mathcal{L}_{\text{SURE}} + \mathcal{L}_{\text{EI}}$ to train. While SURE has been generalised to the case of rank-deficient \mathbf{A} in GSURE [25] and LDAMP-SURE [52, 98], ENSURE [5] is shown to improve on these by attempting to leverage multi-operator information of \mathcal{A} :

$$\mathcal{L}_{\text{ENSURE}} = \|\mathbf{R}(\mathbf{A}^\dagger \mathbf{y} - f_\theta(\mathbf{y}, \mathbf{A}))\|_2^2 + \frac{2\sigma^2}{\tau} \mathbf{b}^\top (f_\theta(\mathbf{A}^\top \mathbf{y} + \tau\mathbf{b}, \mathbf{A}) - f_\theta(\mathbf{A}^\top \mathbf{y})) \quad (15)$$

where $\mathbf{R} = \mathbb{E}[\mathbf{P}]^{-\frac{1}{2}} \mathbf{P}$, $\mathbf{P} = \mathbf{A}^\dagger \mathbf{A}$. Note that when $\sigma \rightarrow 0$, ENSURE simply reduces to \mathcal{L}_{MC} .

SSDU-style methods have also been adapted to the noisy case using Noisier2Noise-style reoccurring losses [55]. Robust-SSDU [54] performs an additional reoccurring $\tilde{\mathbf{y}} \sim \mathcal{N}(\mathbf{y}, \alpha^2 \sigma^2 \mathbf{I})$ and constructs the loss that attempts to remove this:

$$\mathcal{L}_{\text{Robust-SSDU}} = \mathcal{L}_{\text{Weighted-SSDU}}(\tilde{\mathbf{y}}; \mathbf{y}) + \|(1 + \frac{1}{\alpha^2})\mathbf{M}_1 \mathbf{M}(\mathbf{A}f_\theta(\tilde{\mathbf{y}}, \mathbf{A}) - \mathbf{y})\|_2^2 \quad (16)$$

where α is a hyperparameter. Similarly, Noise2Recon-SSDU [23] considers reoccurring as a noising special-case of [22], and appends this to SSDU $\mathcal{L}_{\text{Noise2Recon-SSDU}} = \mathcal{L}_{\text{SSDU}} + \mathcal{L}_{\text{VORTEX}, \mathbf{T}_1=\mathcal{N}, \mathbf{T}_2=\mathbf{I}}$. DDSSL [66] also adds a random noising special-case of $\mathcal{L}_{\text{EI}, \mathbf{T}=\mathcal{N}}$ to Recorruped2Recorruped [63].

2.4 Related work

Surveys for imaging inverse problems Recent surveys exist covering inverse problems with deep learning [60], for MRI reconstruction [33, 15] and without GT [94, 6]. [6, 33, 60] focus on a minimal set of self-supervised methods (*e.g.* one to five) and their subsequent extensions; [15] do not mention any. [94, 6] and works such as [86] lack a principled comparison of the core theoretical differences between methods, comparing instead entire pipelines, conflating therefore mostly orthogonal problems including model architecture f_θ or forward operator \mathbf{A} . Additionally, none of these works are comprehensive. The works of [33, 94, 6] do not provide any experimental results. Previous individual works either do not report comparison with other methods *e.g.* [17, 13], or compare to very few *e.g.* [54, 22, 5], which are inherently limited in scope; a comprehensive benchmark comparison is lacking. Papers commonly do not provide public implementations of competitor methods, potentially reducing the trustworthiness of the comparisons, especially when

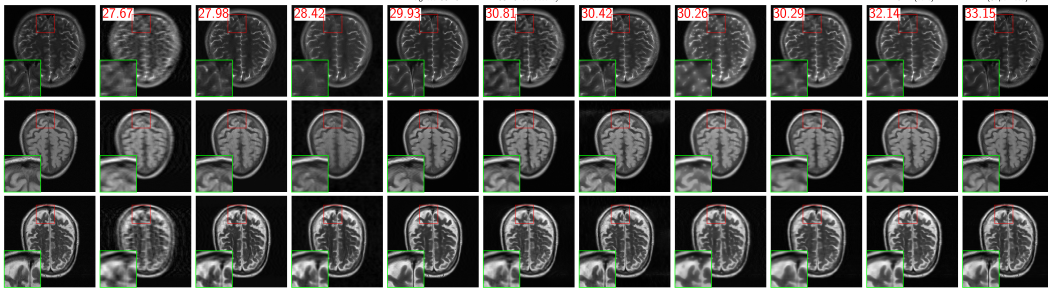


Figure 2: Sample reconstructions for scenario 1 (single-coil noiseless $6\times$ acc.) with average test-set PSNR, showing selected highest-performing methods. See Table 2 for full results.

competitors’ codebases are directly used without disentangling the method from the experimental setup. On the contrary, we highlight the key conceptual difference, the loss function, and benchmark this while keeping constant all other elements of the imaging pipeline, providing empirical results across multiple directly comparable setups. Furthermore, we reimplement the compared methods in a common codebase, bypassing the practical barriers of code uninteroperability, to encourage reproducible future research.

Benchmarks for imaging inverse problems Numerous imaging benchmarks on real data have been proposed for tasks such as MRI [93, 24] or CT [41]. However, to the best of our knowledge, in any domain, no benchmarks on image reconstruction from partial measurements without GT exist.

3 Experimental setup

We evaluate all methods from Table 1 using our reimplementations on the following justified setup:

Data We retrospectively simulate \mathbf{y} from the popular FastMRI brain dataset [93], using the same RSS references for each scenario, in order to fully control the forward operator \mathbf{A} (its distribution is needed for [91, 53, 34, 78]) and have GT \mathbf{x} for evaluation. The specific forward operator \mathbf{A} varies for each benchmarked scenario. For the multi-coil case we assume known coil maps to focus on the reconstruction task and not introduce artifacts associated with map estimation.

Model f_θ From the vast literature [33] we choose an unrolled network architecture, which balances being specific for efficient image reconstruction yet sufficiently general to not favour specific losses. We choose the popular MoDL [4], unrolling finite steps (we use 3 steps) of half-quadratic splitting [96]. Identical hyperparameters are used for all loss functions to provide fair comparisons.

Evaluation We report PSNR and SSIM as used in [93]. For reference baseline comparison, we use the no-learning zero-filled (ZF) $\hat{\mathbf{x}} = \mathbf{A}^\top \mathbf{y}$ instead of the iterative PICS [49] or SENSE $\hat{\mathbf{x}} = \mathbf{A}^\dagger \mathbf{y}$ (in the multi-coil case) [64]. We also train a gold-standard model with the supervised oracle loss $\ell(\hat{\mathbf{x}}, \mathbf{x})$.

We highlight that our modular benchmark framework facilitates replacing any element of the setup used here: other SotA architectures, popular image quality metrics, or forward operator scenarios. Further experimental setup details, annotated loss sketches and training code are in Appendix B. Benchmark code and contribution instructions are at <https://andrewwango.github.io/ssibench>. We also conduct further in-depth experiments: testing performance scaling as unrolling depth increases, robustness to out-of-domain data, and component ablations on MO-EI and SSDU. We also demonstrate the ease of benchmark transferability to an environmental imaging task.

3.1 Results

Scenario 1 (single-coil noiseless) Results are shown in Table 2 and Fig. 2. As expected, MC cannot improve the ZF performance, as it cannot learn information from the null-space; results presented in [70] may instead heavily rely on a specific network’s inductive bias. EI and MOI both show good results but suffer from strong artifacts in the brain images. MO-EI improves significantly on

Loss	PSNR \uparrow	SSIM \uparrow	Loss	PSNR \uparrow	SSIM \uparrow
Zero-filled	27.67 \pm 2.40	.7862 \pm .05	Zero-filled	24.34 \pm 1.01	.4428 \pm .03
MC	27.66 \pm 2.40	.7861 \pm .0550	ENSURE	26.29 \pm 1.51	.5856 \pm .0360
SSDU	27.98 \pm 1.43	.7485 \pm .0667	Robust-SSDU	27.42 \pm 1.13	.6159 \pm .0425
Noise2Inverse	28.42 \pm 2.02	.7853 \pm .0735	Noise2Recon-SSDU	27.84 \pm 1.78	.7661 \pm .0727
Weighted-SSDU	29.93 \pm 1.66	.8355 \pm .0626	DDSSL	28.25 \pm 2.30	.7836 \pm .0547
SSDU-Consistency	30.81 \pm 2.58	.8495 \pm .0581	Robust-EI	29.07 \pm 2.37	.8227 \pm .0578
CC-SSDU	30.42 \pm 2.71	.8198 \pm .0854	Robust-MO-EI	29.72\pm2.44	.8409\pm.0575
Adversarial	18.52 \pm .31	.4732 \pm .0388	Non-robust	26.12 \pm 1.92	.6002 \pm .0602
UAIR	14.00 \pm 1.88	.3715 \pm .0824	MO-EI		
VORTEX	27.75 \pm 2.35	.7898 \pm .0543	Non-robust		
EI	30.26 \pm 2.61	.8523 \pm .0542	Weighted-SSDU	25.91 \pm .94	.5477 \pm .0511
MOI	30.29 \pm 2.88	.8651 \pm .0528	(Supervised)	30.19 \pm 2.10	.8411 \pm .0552
MO-EI (ours)	32.14\pm2.73	.8846\pm.0498			
(Supervised)	33.15 \pm 2.76	.9032 \pm .0435			

Table 2: Test set results (mean and std. dev.) for scenario 1 (single-coil noiseless $6\times$ acc.)

Table 3: Test set results for scenario 2 (noisy $6\times$ accelerated measurements at $\sigma = 0.1$).

Best unsupervised method in bold.

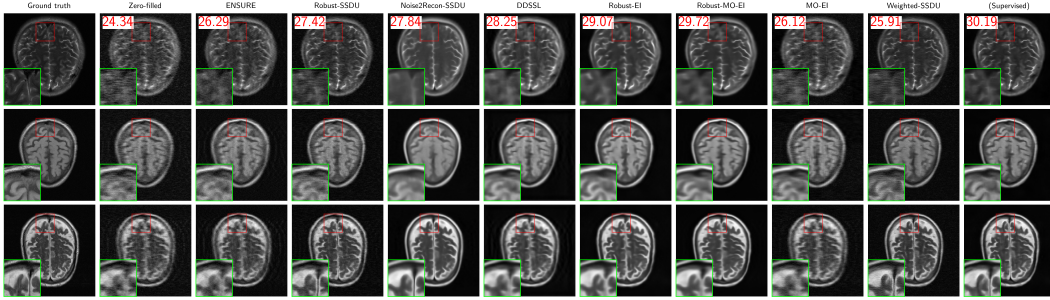


Figure 3: Sample reconstructions for scenario 2 (noisy $6\times$ acc.) with average test-set PSNR.

both these previous SotA methods (see Appendix C.1 for statistical test), approaching the oracle supervised learning performance. SSDU suppresses artifacts and recovers sharper edges quite well, but its quantitative performance is relatively poor, with other methods based on splitting improving on this. We attribute the very poor performance of the adversarial losses to the well-known instability and sensitivity of training f_θ and D [69]: after extensive experimentation we were unable to reproduce the results from [17] (which use a proprietary dataset), which may require heavy hyperparameter tuning and specific architectures. Since UAIR [61] does not show results on accelerated MRI, we assume that their results do not transfer. Finally, VORTEX learns only marginal information compared to MC, showing that data augmentation alone cannot recover information from the null-space.

Scenario 2 (single-coil noisy) Results are shown in Table 3 and Fig. 3. ENSURE denoises a moderate amount, but strong undersampling artifacts remain. Noise2Recon-SSDU and Robust-SSDU perform fairly well, resulting in clearer reconstructions with fairly sharp edges. The SURE-based Robust-EI and Robust-MO-EI methods are almost artifact-free with high metrics, but they struggle with sharper edges. All loss functions without the denoising terms perform poorly as expected.

Scenario 3 (single-operator) Results are shown in Table 4 and Fig. 8. As expected, the best-performing method is EI, which recovers information from the null-space but *without* the assumption that the image set is seen through multiple masks. Interestingly, other methods which do require this assumption still learn some information over the ZF solution, demonstrating the challenge of disentangling actual learning from network inductive bias.

Scenario 4 (multi-coil) Results are shown in Table 5 and Fig. 9. As expected, MC learns the SENSE reconstruction $\mathbf{A}^\dagger \mathbf{y}$. Interestingly, splitting-based methods consistently outperform EI, MOI and MO-EI, with weighted-SSDU approaching supervised learning. Whereas in previous scenarios, splitting methods struggled to recover information from larger null-spaces, here \mathbf{A} has a higher effective rank (analysis in Appendix C.2), which highlights instead their strength on sharp edges.

Loss	PSNR \uparrow	SSIM \uparrow	Loss	PSNR \uparrow	SSIM \uparrow
Zero-filled	28.02 \pm 2.26	.7900 \pm .05	Zero-filled	27.82 \pm 2.41	.7988 \pm .05
MC	28.02 \pm 2.26	.7900 \pm .0496	MC	28.96 \pm 2.59	.8271 \pm .0495
SSDU	21.89 \pm 1.07	.6288 \pm .0510	SSDU	31.47 \pm 2.67	.8705 \pm .0534
Noise2Inverse	24.63 \pm 2.07	.6559 \pm .0676	Noise2Inverse	30.93 \pm 2.65	.8589 \pm .0570
Weighted-SSDU	30.14 \pm 1.64	.8454 \pm .0615	Weighted-SSDU	33.03 \pm 2.36	.8991 \pm .0479
SSDU-Consistency	31.05 \pm 2.50	.8614 \pm .0567	SSDU-Consistency	32.30 \pm 2.58	.8949 \pm .0425
CC-SSDU	27.85 \pm 1.86	.7717 \pm .0833	CC-SSDU	31.80 \pm 2.69	.8761 \pm .0529
Adversarial	26.53 \pm 1.62	.7013 \pm .0370	Adversarial	17.47 \pm 1.93	.6464 \pm .0590
UAIR	18.44 \pm 1.61	.5388 \pm .0542	UAIR	15.26 \pm 2.16	.3453 \pm .0540
VORTEX	28.07 \pm 2.26	.7916 \pm .0507	VORTEX	23.59 \pm 1.17	.5846 \pm .0469
EI	31.99 \pm 2.80	.8806 \pm .0486	EI	31.66 \pm 2.74	.8769 \pm .0494
MOI	31.60 \pm 2.74	.8789 \pm .0477	MOI	31.37 \pm 2.86	.8810 \pm .0502
MO-EI (ours)	31.11 \pm 2.69	.8713 \pm .0496	MO-EI (ours)	31.56 \pm 2.85	.8836 \pm .0477
(Supervised)	34.03 \pm 2.49	.9040 \pm .0435	(Supervised)	33.89 \pm 2.78	.9147 \pm .0365

Table 4: Test set results for scenario 3 ($6\times$ acc. single-operator fixed mask).

Table 5: Test set results for scenario 4 ($6\times$ acc. multi-coil measurements $C = 4$).

Further results Results of further experiments and ablations are shown in Appendix C. Generally, performances of different methods increase uniformly with unrolling depth, suggesting that our results would scale to setups with larger models. Additionally, in experiments where ground-truth could be available, we show that adding a self-supervised loss during training considerably improves robustness to out-of-domain data compared to purely supervised learning.

4 Discussion and Conclusions

Design We close an important gap in self-supervised imaging (SSI) for MRI reconstruction without GT by designing a modular and thorough benchmark, **SSIBench**, that unifies 18 distinct losses from the ML and imaging communities. This systematic comparison is crucial for targeted future research and industrial adoption. We formulate four realistic MRI scenarios that each test different capabilities.

Insights Our extensive experiments on a standardised setup show a wide range in performance, with different methods leading (*e.g.* by 2 dB) on different scenarios and metrics: for example, while MOI and EI achieve almost artifact-free reconstructions and lead in metrics in one scenario, measurement splitting methods seem to recover sharper edges and lead in another. These observations motivate further ML research by exposing the ongoing need for a reliable method that can lead on all scenarios. The benchmark facilitates the systematic combination of loss components to discover more effective configurations such as MO-EI, paving the way for future exploration of even more promising ones.

Limitations In future we aim to include a wider range of datasets *e.g.* raw noisy low-field data [50], other forward operators **A** *e.g.* non-Cartesian sampling and more complex models f_θ [81], clinically meaningful metrics [24, 10], or other realistic MRI subtasks *e.g.* joint coil map estimation [36]. Toward further expansion on these fronts, our modular setup facilitates swapping out any of these components to accommodate diverse research configurations. We demonstrate this capability by extending the benchmark framework beyond MRI and provide a proof-of-concept example benchmarking SSI for a task in environmental imaging in Appendix C.7.

Benchmark resource and outlook We provide easy-to-use reimplementations of all benchmarked losses and a site <https://andrewwango.github.io/ssibench> where researchers can contribute. This lowers the barrier to entry and enables ML researchers and practitioners to a) contribute and compare new ML methods on a standard evaluation framework, and b) rapidly and fairly test these methods on their own setups. We encourage the community to generalise our insights and use our benchmark resource as a blueprint to unlock self-supervised learning for emerging, exciting domains within MRI and beyond, while remaining mindful of potential misuse of high quality images.

References

- [1] Asad Aali, Marius Arvinte, Sidharth Kumar, Yamin I. Arefeen, and Jonathan I. Tamir. GSURE Denoising enables training of higher quality generative priors for accelerated Multi-Coil MRI Reconstruction. *ISMRM 2024*, April 2024.
- [2] Asad Aali, Giannis Daras, Brett Levac, Sidharth Kumar, Alex Dimakis, and Jon Tamir. Ambient Diffusion Posterior Sampling: Solving Inverse Problems with Diffusion Models Trained on Corrupted Data. In *International Conference on Learning Representations*, October 2024.
- [3] Mert Acar, Tolga Çukur, and Ilkay Öksüz. Self-supervised Dynamic MRI Reconstruction. In *Machine Learning for Medical Image Reconstruction*, pages 35–44. Springer International Publishing, 2021. doi: 10.1007/978-3-030-88552-6_4.
- [4] Hemant K. Aggarwal, Merry P. Mani, and Mathews Jacob. MoDL: Model-Based Deep Learning Architecture for Inverse Problems. *IEEE Transactions on Medical Imaging*, 38(2):394–405, February 2019. doi: 10.1109/TMI.2018.2865356.
- [5] Hemant Kumar Aggarwal, Aniket Pramanik, Maneesh John, and Mathews Jacob. ENSURE: A General Approach for Unsupervised Training of Deep Image Reconstruction Algorithms. *IEEE Transactions on Medical Imaging*, 42(4):1133–1144, April 2023. doi: 10.1109/TMI.2022.3224359.
- [6] Mehmet Akçakaya, Burhaneddin Yaman, Hyungjin Chung, and Jong Chul Ye. Unsupervised Deep Learning Methods for Biological Image Reconstruction and Enhancement: An overview from a signal processing perspective. *IEEE Signal Processing Magazine*, 39(2):28–44, March 2022. doi: 10.1109/MSP.2021.3119273.
- [7] Yaşar Utku Alçalar, Merve Gülle, and Mehmet Akçakaya. A Convex Compressibility-Inspired Unsupervised Loss Function for Physics-Driven Deep Learning Reconstruction. In *2024 IEEE International Symposium on Biomedical Imaging (ISBI)*, pages 1–5, May 2024. doi: 10.1109/ISBI56570.2024.10635138.
- [8] Theo Bodrito, Alexandre Zouaoui, Jocelyn Chanussot, and Julien Mairal. A Trainable Spectral-Spatial Sparse Coding Model for Hyperspectral Image Restoration. In *Advances in Neural Information Processing Systems*, volume 34, pages 5430–5442, 2021.
- [9] Ashish Bora, Eric Price, and Alexandros G. Dimakis. AmbientGAN: Generative models from lossy measurements. In *International Conference on Learning Representations*, February 2018.
- [10] Anna Breger, Ander Biguri, Malena Sabaté Landman, Ian Selby, Nicole Amberg, Elisabeth Brunner, Janek Gröhl, Sepideh Hatamikia, Clemens Karner, Lipeng Ning, Sören Dittmer, Michael Roberts, AIX-COVNET Collaboration, and Carola-Bibiane Schönlieb. A study of why we need to reassess full reference image quality assessment with medical images. *Journal of Imaging Informatics in Medicine*, March 2025. doi: 10.1007/s10278-025-01462-1.
- [11] Akshay S. Chaudhari, Christopher M. Sandino, Elizabeth K. Cole, David B. Larson, Garry E. Gold, Shreyas S. Vasanawala, Matthew P. Lungren, Brian A. Hargreaves, and Curtis P. Langlotz. Prospective Deployment of Deep Learning in MRI: A Framework for Important Considerations, Challenges, and Recommendations for Best Practices. *Journal of Magnetic Resonance Imaging*, 54(2):357–371, 2021. doi: 10.1002/jmri.27331.
- [12] Dongdong Chen, Julián Tachella, and Mike E. Davies. Equivariant Imaging: Learning Beyond the Range Space. In *2021 IEEE/CVF International Conference on Computer Vision (ICCV)*, October 2021. doi: 10.1109/ICCV48922.2021.00434.
- [13] Dongdong Chen, Julián Tachella, and Mike E. Davies. Robust Equivariant Imaging: a fully unsupervised framework for learning to image from noisy and partial measurements. In *2022 IEEE/CVF Conference on Computer Vision and Pattern Recognition (CVPR)*, June 2022. doi: 10.1109/CVPR52688.2022.00556.
- [14] Dongdong Chen, Mike Davies, Matthias J. Ehrhardt, Carola-Bibiane Schönlieb, Ferdia Sherry, and Julián Tachella. Imaging With Equivariant Deep Learning: From unrolled network design to fully unsupervised learning. *IEEE Signal Processing Magazine*, 40(1):134–147, January 2023. doi: 10.1109/MSP.2022.3205430.

- [15] Yutong Chen, Carola-Bibiane Schönlieb, Pietro Liò, Tim Leiner, Pier Luigi Dragotti, Ge Wang, Daniel Rueckert, David Firmin, and Guang Yang. AI-Based Reconstruction for Fast MRI—A Systematic Review and Meta-Analysis. *Proceedings of the IEEE*, 110(2):224–245, February 2022. doi: 10.1109/JPROC.2022.3141367.
- [16] Hyungjin Chung and Jong Chul Ye. Score-based diffusion models for accelerated MRI. *Medical Image Analysis*, 80:102479, August 2022. doi: 10.1016/j.media.2022.102479.
- [17] Elizabeth K. Cole, Frank Ong, Shreyas S. Vasanawala, and John M. Pauly. Fast Unsupervised MRI Reconstruction Without Fully-Sampled Ground Truth Data Using Generative Adversarial Networks. In *2021 IEEE/CVF International Conference on Computer Vision Workshops (ICCVW)*, pages 3971–3980, October 2021. doi: 10.1109/ICCVW54120.2021.00444.
- [18] Giannis Daras, Kulin Shah, Yuval Dagan, Aravind Gollakota, Alexandros G. Dimakis, and Adam Klivans. Ambient Diffusion: Learning Clean Distributions from Corrupted Data, May 2023. arXiv:2305.19256 [cs, math].
- [19] Giannis Daras, Hyungjin Chung, Chieh-Hsin Lai, Yuki Mitsufuji, Jong Chul Ye, Peyman Milanfar, Alexandros G. Dimakis, and Mauricio Delbracio. A Survey on Diffusion Models for Inverse Problems, September 2024. arXiv:2410.00083 [cs].
- [20] Mohammad Zalbagi Darestani and Reinhard Heckel. Accelerated MRI with Un-trained Neural Networks, April 2021. arXiv:2007.02471 [eess].
- [21] Mohammad Zalbagi Darestani, Jiayu Liu, and Reinhard Heckel. Test-Time Training Can Close the Natural Distribution Shift Performance Gap in Deep Learning Based Compressed Sensing. In *Proceedings of the 39th International Conference on Machine Learning*, pages 4754–4776. PMLR, June 2022.
- [22] Arjun D. Desai, Beliz Gunel, Batu M. Ozturkler, Harris Beg, Shreyas Vasanawala, Brian A. Hargreaves, Christopher Ré, John M. Pauly, and Akshay S. Chaudhari. VORTEX: Physics-Driven Data Augmentations Using Consistency Training for Robust Accelerated MRI Reconstruction, June 2022. arXiv:2111.02549 [eess].
- [23] Arjun D. Desai, Batu M. Ozturkler, Christopher M. Sandino, Robert Boutin, Marc Willis, Shreyas Vasanawala, Brian A. Hargreaves, Christopher M. Ré, John M. Pauly, and Akshay S. Chaudhari. Noise2Recon: Enabling Joint MRI Reconstruction and Denoising with Semi-Supervised and Self-Supervised Learning, October 2022. arXiv:2110.00075 [eess].
- [24] Arjun D. Desai, Andrew M. Schmidt, Elka B. Rubin, Christopher M. Sandino, Marianne S. Black, Valentina Mazzoli, Kathryn J. Stevens, Robert Boutin, Christopher Ré, Garry E. Gold, Brian A. Hargreaves, and Akshay S. Chaudhari. SKM-TEA: A Dataset for Accelerated MRI Reconstruction with Dense Image Labels for Quantitative Clinical Evaluation, March 2022. arXiv:2203.06823 [eess].
- [25] Yonina C. Eldar. Generalized SURE for Exponential Families: Applications to Regularization. *IEEE Transactions on Signal Processing*, 57(2):471–481, February 2009. doi: 10.1109/TSP.2008.2008212.
- [26] Linus Ericsson, Henry Gouk, and Timothy M. Hospedales. Why Do Self-Supervised Models Transfer? Investigating the Impact of Invariance on Downstream Tasks, October 2022. arXiv:2111.11398 [cs].
- [27] Linus Ericsson, Henry Gouk, Chen Change Loy, and Timothy M. Hospedales. Self-Supervised Representation Learning: Introduction, advances, and challenges. *IEEE Signal Processing Magazine*, 39(3):42–62, May 2022. doi: 10.1109/MSP.2021.3134634.
- [28] Zalan Fabian, Reinhard Heckel, and Mahdi Soltanolkotabi. Data augmentation for deep learning based accelerated MRI reconstruction with limited data. In *Proceedings of the 38th International Conference on Machine Learning*, pages 3057–3067, July 2021.

- [29] Oren Freifeld, Søren Hauberg, Kayhan Batmanghelich, and Jonn W. Fisher. Transformations Based on Continuous Piecewise-Affine Velocity Fields. *IEEE Transactions on Pattern Analysis and Machine Intelligence*, 39(12):2496–2509, December 2017. doi: 10.1109/TPAMI.2016.2646685.
- [30] Weijie Gan, Yu Sun, Cihat Eldeniz, Jiaming Liu, Hongyu An, and Ulugbek S. Kamilov. Deep Image Reconstruction Using Unregistered Measurements Without Groundtruth. In *2021 IEEE 18th International Symposium on Biomedical Imaging (ISBI)*, pages 1531–1534, April 2021. doi: 10.1109/ISBI48211.2021.9434079.
- [31] Weijie Gan, Yu Sun, Cihat Eldeniz, Jiaming Liu, Hongyu An, and Ulugbek S. Kamilov. Deformation-Compensated Learning for Image Reconstruction Without Ground Truth. *IEEE Transactions on Medical Imaging*, 41(9):2371–2384, September 2022. ISSN 1558-254X. doi: 10.1109/TMI.2022.3163018.
- [32] Zhuonan He, Cong Quan, Siyuan Wang, Yuanzheng Zhu, Minghui Zhang, Yanjie Zhu, Qiegen Liu, Zhuonan He, Cong Quan, Siyuan Wang, Yuanzheng Zhu, Minghui Zhang, Yanjie Zhu, and Qiegen Liu. A Comparative Study of Unsupervised Deep Learning Methods for MRI Reconstruction. *Investigative Magnetic Resonance Imaging*, pages 179–195, 2020.
- [33] Reinhard Heckel, Mathews Jacob, Akshay Chaudhari, Or Perlmán, and Efrat Shimron. Deep learning for accelerated and robust MRI reconstruction. *Magnetic Resonance Materials in Physics, Biology and Medicine*, 37(3):335–368, July 2024. doi: 10.1007/s10334-024-01173-8.
- [34] Allard Adriaan Hendriksen, Daniël Maria Pelt, and K. Joost Batenburg. Noise2Inverse: Self-Supervised Deep Convolutional Denoising for Tomography. *IEEE Transactions on Computational Imaging*, 6:1320–1335, 2020. doi: 10.1109/TCI.2020.3019647.
- [35] Chen Hu, Cheng Li, Haifeng Wang, Qiegen Liu, Hairong Zheng, and Shanshan Wang. Self-supervised Learning for MRI Reconstruction with a Parallel Network Training Framework. In Marleen de Bruijne, Philippe C. Cattin, Stéphane Cotin, Nicolas Padoy, Stefanie Speidel, Yefeng Zheng, and Caroline Essert, editors, *Medical Image Computing and Computer Assisted Intervention – MICCAI 2021*, pages 382–391, 2021. doi: 10.1007/978-3-030-87231-1_37.
- [36] Yuyang Hu, Weijie Gan, Chunwei Ying, Tongyao Wang, Cihat Eldeniz, Jiaming Liu, Yasheng Chen, Hongyu An, and Ulugbek S. Kamilov. SPICER: Self-Supervised Learning for MRI with Automatic Coil Sensitivity Estimation and Reconstruction, June 2024. arXiv:2210.02584 [eess].
- [37] Peizhou Huang, Chaoyi Zhang, Hongyu Li, Sunil Kumar Gaire, Ruiying Liu, Xiaoliang Zhang, Xiaojuan Li, and Leslie Ying. Deep MRI Reconstruction without Ground Truth for Training. In *Proc. Intl. Soc. Mag. Reson. Med.* 27, 2019.
- [38] Peizhou Huang, Chaoyi Zhang, Xiaoliang Zhang, Xiaojuan Li, Liang Dong, and Leslie Ying. Self-Supervised Deep Unrolled Reconstruction Using Regularization by Denoising. *IEEE Transactions on Medical Imaging*, 43(3):1203–1213, March 2024. doi: 10.1109/TMI.2023.3332614.
- [39] Nikola Janjušević, Jingjia Chen, Luke Ginocchio, Mary Bruno, Yuhui Huang, Yao Wang, Hersh Chandarana, and Li Feng. Self-Supervised Noise Adaptive MRI Denoising via Repetition to Repetition (Rep2Rep) Learning, April 2025. arXiv:2504.17698 [eess].
- [40] Bahjat Kavar, Noam Elata, Tomer Michaeli, and Michael Elad. GSURE-Based Diffusion Model Training with Corrupted Data, June 2024. arXiv:2305.13128 [eess].
- [41] Maximilian B. Kiss, Ander Biguri, Zakhar Shumaylov, Ferdia Sherry, K. Joost Batenburg, Carola-Bibiane Schönlieb, and Felix Lucka. Benchmarking learned algorithms for computed tomography image reconstruction tasks. *Applied Mathematics for Modern Challenges*, 3(0): 1–43, February 2025. doi: 10.3934/ammc.2025001.
- [42] Tobit Klug, Dogukan Atik, and Reinhard Heckel. Analyzing the Sample Complexity of Self-Supervised Image Reconstruction Methods. *Advances in Neural Information Processing Systems*, 36:65869–65893, December 2023.

- [43] Yilmaz Korkmaz, Salman U. H. Dar, Mahmut Yurt, Muzaffer Özbey, and Tolga Çukur. Unsupervised MRI Reconstruction via Zero-Shot Learned Adversarial Transformers. *IEEE Transactions on Medical Imaging*, 41(7):1747–1763, July 2022. doi: 10.1109/TMI.2022.3147426.
- [44] Ke Lei, Morteza Mardani, John M. Pauly, and Shreyas S. Vasanawala. Wasserstein GANs for MR Imaging: From Paired to Unpaired Training. *IEEE Transactions on Medical Imaging*, 40(1):105–115, January 2021. doi: 10.1109/TMI.2020.3022968.
- [45] Bowen Li, Zhiwen Wang, Ziyuan Yang, Wenjun Xia, and Yi Zhang. Progressive dual-domain-transfer cycleGAN for unsupervised MRI reconstruction. *Neurocomputing*, 563:126934, January 2024. doi: 10.1016/j.neucom.2023.126934.
- [46] Jiaming Liu, Yu Sun, Cihat Eldeniz, Weijie Gan, Hongyu An, and Ulugbek S. Kamilov. RARE: Image Reconstruction Using Deep Priors Learned Without Groundtruth. *IEEE Journal of Selected Topics in Signal Processing*, 14(6):1088–1099, October 2020. doi: 10.1109/JSTSP.2020.2998402.
- [47] Mario Lucic, Karol Kurach, Marcin Michalski, Sylvain Gelly, and Olivier Bousquet. Are GANs Created Equal? A Large-Scale Study. In *Advances in Neural Information Processing Systems*, 2018.
- [48] Xinzhe Luo, Yingzhen Li, and Chen Qin. Unsupervised Accelerated MRI Reconstruction via Ground-Truth-Free Flow Matching, February 2025. arXiv:2502.17174 [eess].
- [49] Michael Lustig, David L. Donoho, Juan M. Santos, and John M. Pauly. Compressed Sensing MRI. *IEEE Signal Processing Magazine*, 25(2):72–82, March 2008. doi: 10.1109/MSP.2007.914728.
- [50] Mengye Lyu, Lifeng Mei, Shoujin Huang, Sixing Liu, Yi Li, Kexin Yang, Yilong Liu, Yu Dong, Linzheng Dong, and Ed X. Wu. M4Raw: A multi-contrast, multi-repetition, multi-channel MRI k-space dataset for low-field MRI research. *Scientific Data*, 10(1):264, May 2023. doi: 10.1038/s41597-023-02181-4.
- [51] Xiangchao Meng, Yiming Xiong, Feng Shao, Huanfeng Shen, Weiwei Sun, Gang Yang, Qiangqiang Yuan, Randi Fu, and Hongyan Zhang. A Large-Scale Benchmark Data Set for Evaluating Pansharpening Performance: Overview and Implementation. *IEEE Geoscience and Remote Sensing Magazine*, March 2021. doi: 10.1109/MGRS.2020.2976696.
- [52] Christopher A. Metzler, Ali Mousavi, Reinhard Heckel, and Richard G. Baraniuk. Unsupervised Learning with Stein’s Unbiased Risk Estimator, July 2020. arXiv:1805.10531 [stat].
- [53] Charles Millard and Mark Chiew. A Theoretical Framework for Self-Supervised MR Image Reconstruction Using Sub-Sampling via Variable Density Noisier2Noise. *IEEE Transactions on Computational Imaging*, 9:707–720, 2023. doi: 10.1109/TCI.2023.3299212.
- [54] Charles Millard and Mark Chiew. Clean self-supervised MRI reconstruction from noisy, sub-sampled training data with Robust SSDU, June 2024. arXiv:2210.01696 [eess].
- [55] Nick Moran, Dan Schmidt, Yu Zhong, and Patrick Coady. Noisier2Noise: Learning to Denoise from Unpaired Noisy Data, October 2019. arXiv:1910.11908 [cs, eess].
- [56] Subhadip Mukherjee, Marcello Carioni, Ozan Öktem, and Carola-Bibiane Schönlieb. End-to-end reconstruction meets data-driven regularization for inverse problems. In *Advances in Neural Information Processing Systems*, volume 34, pages 21413–21425, 2021.
- [57] Gyutaek Oh, Byeongsu Sim, HyungJin Chung, Leonard Sunwoo, and Jong Chul Ye. Unpaired Deep Learning for Accelerated MRI Using Optimal Transport Driven CycleGAN. *IEEE Transactions on Computational Imaging*, 6:1285–1296, 2020. doi: 10.1109/TCI.2020.3018562.
- [58] Frank Ong and Michael Lustig. SigPy: a python package for high performance iterative reconstruction. In *Proceedings of the ISMRM 27th Annual Meeting, Montreal, Quebec, Canada*, volume 4819, 2019.

- [59] Frank Ong, Xucheng Zhu, Joseph Y. Cheng, Kevin M. Johnson, Peder E. Z. Larson, Shreyas S. Vasanawala, and Michael Lustig. Extreme MRI: Large-scale volumetric dynamic imaging from continuous non-gated acquisitions. *Magnetic Resonance in Medicine*, 84(4):1763–1780, 2020. doi: 10.1002/mrm.28235.
- [60] Gregory Ongie, Ajil Jalal, Christopher A. Metzler, Richard G. Baraniuk, Alexandros G. Dimakis, and Rebecca Willett. Deep Learning Techniques for Inverse Problems in Imaging. *IEEE Journal on Selected Areas in Information Theory*, 1(1):39–56, May 2020. doi: 10.1109/JSAIT.2020.2991563.
- [61] Arthur Pajot, Emmanuel de Bezenac, and Patrick Gallinari. Unsupervised Adversarial Image Reconstruction. In *International Conference on Learning Representations*, September 2018.
- [62] Li Pang, Xiangyu Rui, Long Cui, Hongzhong Wang, Deyu Meng, and Xiangyong Cao. HIR-Diff: Unsupervised Hyperspectral Image Restoration Via Improved Diffusion Models. In *Proceedings of the IEEE/CVF Conference on Computer Vision and Pattern Recognition*, pages 3005–3014, 2024.
- [63] Tongyao Pang, Huan Zheng, Yuhui Quan, and Hui Ji. Recorrupted-to-Recorrupted: Unsupervised Deep Learning for Image Denoising. In *Proceedings of the IEEE/CVF Conference on Computer Vision and Pattern Recognition*, pages 2043–2052, 2021.
- [64] Klaas P. Pruessmann, Markus Weiger, Markus B. Scheidegger, and Peter Boesiger. SENSE: Sensitivity encoding for fast MRI. *Magnetic Resonance in Medicine*, 42(5):952–962, 1999. doi: 10.1002/(SICI)1522-2594(199911)42:5<952::AID-MRM16>3.0.CO;2-S.
- [65] Xinran Qin, Yuhui Quan, Tongyao Pang, and Hui Ji. Ground-Truth Free Meta-Learning for Deep Compressive Sampling. In *Proceedings of the IEEE/CVF Conference on Computer Vision and Pattern Recognition*, pages 9947–9956, 2023.
- [66] Yuhui Quan, Xinran Qin, Tongyao Pang, and Hui Ji. Dual-Domain Self-supervised Learning and Model Adaption for Deep Compressive Imaging. In Shai Avidan, Gabriel Brostow, Moustapha Cissé, Giovanni Maria Farinella, and Tal Hassner, editors, *Computer Vision – ECCV 2022*, pages 409–426, Cham, 2022. Springer Nature Switzerland. doi: 10.1007/978-3-031-20056-4_24.
- [67] Sathish Ramani, Thierry Blu, and Michael Unser. Monte-Carlo Sure: A Black-Box Optimization of Regularization Parameters for General Denoising Algorithms. *IEEE Transactions on Image Processing*, 17(9):1540–1554, September 2008. doi: 10.1109/TIP.2008.2001404.
- [68] Olaf Ronneberger, Philipp Fischer, and Thomas Brox. U-Net: Convolutional Networks for Biomedical Image Segmentation. In Nassir Navab, Joachim Hornegger, William M. Wells, and Alejandro F. Frangi, editors, *Medical Image Computing and Computer-Assisted Intervention – MICCAI 2015*, pages 234–241, 2015. doi: 10.1007/978-3-319-24574-4_28.
- [69] Tim Salimans, Ian Goodfellow, Wojciech Zaremba, Vicki Cheung, Alec Radford, Xi Chen, and Xi Chen. Improved Techniques for Training GANs. In *Advances in Neural Information Processing Systems*, volume 29. Curran Associates, Inc., 2016.
- [70] Ortal Senouf, Sanketh Vedula, Tomer Weiss, Alex Bronstein, Oleg Michailovich, and Michael Zibulevsky. Self-supervised Learning of Inverse Problem Solvers in Medical Imaging. In Qian Wang, Fausto Milletari, Hien V. Nguyen, Shadi Albarqouni, M. Jorge Cardoso, Nicola Rieke, Ziyue Xu, Konstantinos Kamnitsas, Vishal Patel, Badri Roysam, Steve Jiang, Kevin Zhou, Khoa Luu, and Ngan Le, editors, *Domain Adaptation and Representation Transfer and Medical Image Learning with Less Labels and Imperfect Data*, pages 111–119, Cham, 2019. Springer International Publishing. doi: 10.1007/978-3-030-33391-1_13.
- [71] Muhammad Shafique, Sizhuo Liu, Philip Schniter, and Rizwan Ahmad. MRI Recovery with Self-Calibrated Denoisers without Fully-Sampled Data. *Magnetic Resonance Materials in Physics, Biology and Medicine*, 38(1):53–66, October 2024. doi: 10.1007/s10334-024-01207-1.

- [72] Liyue Shen, John Pauly, and Lei Xing. NeRP: Implicit Neural Representation Learning With Prior Embedding for Sparsely Sampled Image Reconstruction. *IEEE Transactions on Neural Networks and Learning Systems*, 35(1):770–782, January 2024. doi: 10.1109/TNNLS.2022.3177134.
- [73] Efrat Shimron, Jonathan I. Tamir, Ke Wang, and Michael Lustig. Implicit data crimes: Machine learning bias arising from misuse of public data. *Proceedings of the National Academy of Sciences*, 119(13), March 2022. doi: 10.1073/pnas.2117203119.
- [74] Oleksii Sidorov and Jon Yngve Hardeberg. Deep Hyperspectral Prior: Single-Image Denoising, Inpainting, Super-Resolution. In *2019 IEEE/CVF International Conference on Computer Vision Workshop (ICCVW)*, pages 3844–3851, October 2019. doi: 10.1109/ICCVW.2019.00477.
- [75] Anuroop Sriram, Jure Zbontar, Tullie Murrell, Aaron Defazio, C. Lawrence Zitnick, Nafissa Yakubova, Florian Knoll, and Patricia Johnson. End-to-End Variational Networks for Accelerated MRI Reconstruction. In Anne L. Martel, Purang Abolmaesumi, Danail Stoyanov, Diana Mateus, Maria A. Zuluaga, S. Kevin Zhou, Daniel Racoceanu, and Leo Joskowicz, editors, *Medical Image Computing and Computer Assisted Intervention – MICCAI 2020*, pages 64–73, Cham, 2020. Springer International Publishing. ISBN 978-3-030-59713-9. doi: 10.1007/978-3-030-59713-9_7.
- [76] Charles M. Stein. Estimation of the Mean of a Multivariate Normal Distribution. *The Annals of Statistics*, 9(6):1135–1151, November 1981. doi: 10.1214/aos/1176345632.
- [77] Julian Tachella, Dongdong Chen, Samuel Hurault, Matthieu Terris, and Andrew Wang. Deep-Inverse: A deep learning framework for inverse problems in imaging, June 2023. URL <https://github.com/deepinv/deepinv>.
- [78] Julián Tachella, Dongdong Chen, and Mike Davies. Unsupervised Learning From Incomplete Measurements for Inverse Problems. *Advances in Neural Information Processing Systems*, 35: 4983–4995, December 2022.
- [79] Julián Tachella, Mike Davies, and Laurent Jacques. UNSURE: self-supervised learning with Unknown Noise level and Stein’s Unbiased Risk Estimate, February 2025. arXiv:2409.01985 [stat].
- [80] Jonathan I. Tamir, Stella X. Yu, and Michael Lustig. Unsupervised Deep Basis Pursuit: Learning inverse problems without ground-truth data, February 2020. arXiv:1910.13110 [eess].
- [81] Asma Tanabene, Chaithya Giliyar Radhakrishna, Aurélien Massire, Mariappan S. Nadar, and Philippe Ciuciu. Benchmarking 3D multi-coil NC-PDNet MRI reconstruction, November 2024. arXiv:2411.05883 [eess].
- [82] Shashanka Ubaru and Yousef Saad. Fast methods for estimating the Numerical rank of large matrices. In *Proceedings of The 33rd International Conference on Machine Learning*, pages 468–477. PMLR, June 2016.
- [83] Alan Q. Wang, Adrian V. Dalca, and Mert R. Sabuncu. Neural Network-Based Reconstruction in Compressed Sensing MRI Without Fully-Sampled Training Data. In Farah Deeba, Patricia Johnson, Tobias Würfl, and Jong Chul Ye, editors, *Machine Learning for Medical Image Reconstruction*, pages 27–37, 2020. ISBN 978-3-030-61598-7. doi: 10.1007/978-3-030-61598-7_3.
- [84] Andrew Wang and Mike Davies. Fully Unsupervised Dynamic MRI Reconstruction via Diffeo-Temporal Equivariance, October 2024. arXiv:2410.08646 [eess].
- [85] Andrew Wang and Mike Davies. Perspective-Equivariance for Unsupervised Imaging with Camera Geometry, March 2024. arXiv:2403.09327 [cs, eess].
- [86] Frederic Wang, Han Qi, Alfredo De Goyeneche, Reinhard Heckel, Michael Lustig, and Efrat Shimron. K-band: Self-supervised MRI Reconstruction via Stochastic Gradient Descent over K-space Subsets, May 2024. arXiv:2308.02958 [eess].

- [87] Shanshan Wang, Ruoyou Wu, Cheng Li, Juan Zou, Ziyao Zhang, Qiegen Liu, Yan Xi, and Hairong Zheng. PARCEL: Physics-Based Unsupervised Contrastive Representation Learning for Multi-Coil MR Imaging. *IEEE/ACM Transactions on Computational Biology and Bioinformatics*, 20(5):2659–2670, September 2023. doi: 10.1109/TCBB.2022.3213669.
- [88] Zhihao Xia and Ayan Chakrabarti. Training Image Estimators without Image Ground Truth. In *Advances in Neural Information Processing Systems*, volume 32, 2019.
- [89] Qizhe Xie, Zihang Dai, Eduard Hovy, Minh-Thang Luong, and Quoc V. Le. Unsupervised Data Augmentation for Consistency Training, November 2020. arXiv:1904.12848 [cs].
- [90] Burhaneddin Yaman, Seyed Amir Hossein Hosseini, Steen Moeller, Jutta Ellermann, Kâmil Uğurbil, and Mehmet Akçakaya. Self-supervised learning of physics-guided reconstruction neural networks without fully sampled reference data. *Magnetic Resonance in Medicine*, 84(6):3172–3191, 2020. doi: 10.1002/mrm.28378.
- [91] Burhaneddin Yaman, Hongyi Gu, Seyed Amir Hossein Hosseini, Omer Burak Demirel, Steen Moeller, Jutta Ellermann, Kâmil Uğurbil, and Mehmet Akçakaya. Multi-mask self-supervised learning for physics-guided neural networks in highly accelerated magnetic resonance imaging. *NMR in Biomedicine*, 35(12):e4798, 2022. doi: 10.1002/nbm.4798.
- [92] Burhaneddin Yaman, Seyed Amir Hossein Hosseini, and Mehmet Akçakaya. Zero-Shot Self-Supervised Learning for MRI Reconstruction. In *International Conference on Learning Representations*, January 2022.
- [93] Jure Zbontar, Florian Knoll, Anuroop Sriram, Tullie Murrell, Zhengnan Huang, Matthew J. Muckley, Aaron Defazio, Ruben Stern, Patricia Johnson, Mary Bruno, Marc Parente, Krzysztof J. Geras, Joe Katsnelson, Hersh Chandarana, Zizhao Zhang, Michal Drozdal, Adriana Romero, Michael Rabbat, Pascal Vincent, Nafissa Yakubova, James Pinkerton, Duo Wang, Erich Owens, C. Lawrence Zitnick, Michael P. Recht, Daniel K. Sodickson, and Yvonne W. Lui. fastMRI: An Open Dataset and Benchmarks for Accelerated MRI, November 2018. URL <https://arxiv.org/abs/1811.08839v2>.
- [94] Gushan Zeng, Yi Guo, Jiaying Zhan, Zi Wang, Zongying Lai, Xiaofeng Du, Xiaobo Qu, and Di Guo. A review on deep learning MRI reconstruction without fully sampled k-space. *BMC Medical Imaging*, 21(1):195, December 2021. doi: 10.1186/s12880-021-00727-9.
- [95] Chi Zhang, Omer Burak Demirel, and Mehmet Akçakaya. Cycle-Consistent Self-Supervised Learning for Improved Highly-Accelerated MRI Reconstruction. In *2024 IEEE International Symposium on Biomedical Imaging (ISBI)*, pages 1–5, May 2024. doi: 10.1109/ISBI56570.2024.10635895.
- [96] Kai Zhang, Yawei Li, Wangmeng Zuo, Lei Zhang, Luc Van Gool, and Radu Timofte. Plug-and-Play Image Restoration With Deep Denoiser Prior. *IEEE Transactions on Pattern Analysis and Machine Intelligence*, 44(10):6360–6376, October 2022. doi: 10.1109/TPAMI.2021.3088914.
- [97] Bo Zhou, Jo Schlemper, Neel Dey, Seyed Sadegh Mohseni Salehi, Kevin Sheth, Chi Liu, James S. Duncan, and Michal Sofka. Dual-domain self-supervised learning for accelerated non-Cartesian MRI reconstruction. *Medical Image Analysis*, 81:102538, October 2022. doi: 10.1016/j.media.2022.102538.
- [98] Magauyiya Zhussip, Shakarim Soltanayev, and Se Young Chun. Training Deep Learning Based Image Denoisers From Undersampled Measurements Without Ground Truth and Without Image Prior. In *2019 IEEE/CVF Conference on Computer Vision and Pattern Recognition (CVPR)*, pages 10247–10256, June 2019. doi: 10.1109/CVPR.2019.01050.
- [99] Qing Zou, Abdul Haseeb Ahmed, Prashant Nagpal, Stanley Kruger, and Mathews Jacob. Dynamic Imaging Using a Deep Generative STORM (Gen-STORM) Model. *IEEE Transactions on Medical Imaging*, 40(11):3102–3112, November 2021. doi: 10.1109/TMI.2021.3065948.

Supplementary Material

A Scope

We exemplify and justify excluded ground-truth free methods from the scope of our benchmark:

1. We **do** consider feedforward methods. We **do not** consider alternative methods that require lengthy inference-time iterative procedures with large NFEs N per image, including Deep Image Prior methods [20, 43, 99] (typically $N \sim 10^{3 \text{ to } 4}$), generative models *e.g.* AmbientGAN [9] ($N \sim 10^{2 \text{ to } 3}$), diffusion methods [18, 40, 2] (typically $N \sim 10^{3 \text{ to } 4}$), implicit neural representation methods [72] ($N = 10^3$), plug-and-play methods using self-supervised denoiser training *e.g.* [71] ($N \sim 10^2$), or test-time training [65, 21] ($N \sim 10^2$). While N is high for all of the above, [48] showed very recently that this could be decreased, and we will consider this in future work.
2. We **do** only consider methods requiring no GT (*i.e.* only require $\{\mathbf{y}_i\}$). We **do not** consider “self-supervised learning” from the literatures of diffusion or other generative models [19, 16] or representation learning [27, 26, 32], all of which require GT images $\{\mathbf{x}_i\}$ while training. We also **do not** consider other situations requiring GT including unpaired data $\{\mathbf{x}_i\}, \{\mathbf{y}_j\}$ [57, 45, 44, 56] or weakly/semi-supervised learning $\{\mathbf{x}_i, \mathbf{y}_i\}, \{\mathbf{y}_j\}$ [22].
3. We **do** consider methods which are generalisable across different model architectures, where the loss function is the conceptual advance [12, 53]. We **do not** consider methods that rely on the inductive bias of very specific architectures [20, 43, 80] and therefore limit the applicability of our benchmark to models of the future.

Note that for joint reconstruction and denoising in noisy measurements $\sigma > 0$, we do not consider methods which perform separate denoising and reconstruction steps [1].

B Further experimental details

B.1 Data preprocessing details

We use a subset of the FastMRI [93] dataset for our experiments, and our dataset is reproducible by following the instructions given on the benchmark website. We take the middle slice of 455 brain volumes, use the provided 320×320 root-sum-square reconstructions as GT, normalise them to $[0, 1]$ and retrospectively simulate measurements using an undersampled Fourier transform using the DeepInverse library [77]². We randomly create train-test datasets with 80-20 split, since the original FastMRI test set does not have GT for evaluation. For the subsampling masks $\mathbf{M}_i \sim \mathcal{M}$, we use random 1D Gaussian masking with $6\times$ acceleration and 8% autocalibration (ACS) lines kept in the centre. For the noisy scenario we add i.i.d. Gaussian measurement noise with $\sigma = 0.1$, and for the single-operator scenario we fix one $\mathbf{M} \sim \mathcal{M}$. For the multi-coil scenario we assume known sensitivity coil maps to decouple the parameter estimation problem from reconstruction, and assume a fixed number of coils C so that the number of measurements m is constant over the dataset. This is necessary as coil sensitivity estimation introduces its own artifacts, particularly in low image-density areas outside the main region of interest, which we do not wish to introduce into our setup. Therefore, we simulate coil maps using sigpy [58] with $C = 4$ and simulate measurements using Eq. (1).

Note that while retrospective simulation is necessary for a controlled benchmarking experiment, future experiments would evaluate benchmarked methods on prospectively acquired data [73, 11].

Note that all images are normalised to the range $[0, 1]$ before plotting.

B.2 Model and hyperparameter details

The unrolled network f_θ unrolls the iterative bi-level optimisation problem provided by half-quadratic splitting [96] for u iterations, originally proposed for MRI in [4], and we take $u = 3$. During inference, this model f_θ requires u forward passes. For the denoiser of our unrolled network, we use a residual U-Net [68] with no batch norm of depth 4, with a total of 8.6M parameters. We train

²<https://deepinv.github.io>

with the Adam optimiser at $1e-3$ learning rate, although we step this per method down to $1e-5$ to achieve convergence. All models are trained with batch size of 4 using 1 NVIDIA GeForce RTX 3090, taking around 15GB memory, with an average training time of 6 hours. Average training time per batch is 0.5s, and average inference time of the trained models f_θ is 0.1s per batch.

B.3 Individual loss implementation details

We provide details of the benchmarked loss functions’ reimplementations below. All components of our modular experiments are implemented using DeepInverse [77]. We provide annotated loss and training code in Appendices B.3.1 and B.4 and full code at <https://andrewwango.github.io/ssibench>.

General notes Some losses compute additional forward passes of f_θ per training iteration. For these, more Monte Carlo passes per iteration could improve performance but we uniformly limit this to one additional pass for all methods for efficiency. Secondly, the training metric ℓ in benchmarked methods’ original papers varies between L1 and L2 (MSE); since this is not instrumental in recovering information, and many methods’ theory rely on the MSE, we use L2 for standardised evaluation. Thirdly, where there is more than one term in the loss we weight the terms evenly.

Measurement consistency: We simply take ℓ as the MSE in kspace as per [70] with $\beta > 0, \alpha = \gamma = 0$. In the multi-coil case, we take ℓ as the MSE in the backprojected \mathbf{A}^\top space as we find this provides better results.

Measurement splitting: We use a 2D mask with split ratio $\rho = 0.6$ following [90], drawn randomly each instance during training following [91]. For weighted-SSDU we use an independent 1D Gaussian mask following [53]. At inference time, we do not perform additional correction for both [53, 54] since our network maps directly to images $f_\theta : \mathcal{Y} \rightarrow \mathcal{X}$. We ablate and justify the splitting mask choices in Appendix C.5.2. For [35], the authors train two networks, but we follow their ablation and share these weights to keep the number of parameters constant for a fair setup, follow the partitioning used above, and remove the ISTA-Net-specific loss terms. Note that [87] is equivalent to the above but takes the consistency loss on embeddings of $\hat{\mathbf{x}}_1, \hat{\mathbf{x}}_2$ instead. Both [87, 97] are equivalent to the above but with the addition of a superfluous \mathcal{L}_{MC} .

Proposition (Equivalence of unpaired Artifact2Artifact as sum of SSDU losses). Consider the Artifact2Artifact [46] scenario where $\mathbf{y}_i^{(k)}$ are independent sets of measurements of the same subject i (e.g. arriving in a stream) such that $\mathbf{y}_i = \bigcup_k \mathbf{y}_i^{(k)} \in \mathbb{R}^m$ is the full undersampled measurement from one acquisition i (i.e. there are no more measurements of the same subject). $\mathbf{A}_i^{(k)\top} \mathbf{y}_i^{(k)}$ are then the independent “artifact”-corrupted images. The Artifact2Artifact loss draws a pair k, l randomly at each iteration and constructs the loss

$$\mathcal{L}_{A2A}^{(k,l)} = \ell(\mathbf{A}_i^{(l)} f_\theta(\mathbf{y}_i^{(k)}, \mathbf{A}_i^{(k)}), \mathbf{y}_i^{(l)}),$$

where $\mathbf{A}_i^{(k)}, \mathbf{A}_i^{(l)}$ are the operators associated with each measurement. We can then write this as the overlapping SSDU loss [90, Fig. 5] by setting $\mathbf{A}_i^{(k)} = \mathbf{M}_k \mathbf{A}_i, \mathbf{A}_i^{(l)} = \mathbf{M}_l \mathbf{A}_i, \mathbf{y}_i^{(k)} = \mathbf{M}_k \mathbf{y}_i, \mathbf{y}_i^{(l)} = \mathbf{M}_l \mathbf{y}_i$ where $\mathbf{M}_k, \mathbf{M}_l$ are two overlapping mask subsampling sets. Then

$$\mathcal{L}_{A2A} = \sum_k \sum_{l \neq k} \mathcal{L}_{SSDU}^{(k,l)}.$$

Learning from invariance For losses involving equivariant imaging, we draw randomly a group transform at each iteration; for rotation we define the group as $G = \text{SO}(\mathbb{R}^2)$ following [12].

Data augmentation For VORTEX [22], noting that the results of their various variants are very similar, for \mathbf{T}_1 we use random noise and their random phase errors with $\sigma = \alpha = 1$ and for \mathbf{T}_2 we use random maximum $\pm 10\%$ shifts and random $\pm 15^\circ$ rotations. We also observe reduced performance when adding more transformations including full $\pm 360^\circ$ rotation, scaling, or shearing. We do not perform curriculum learning as the original paper does not suggest it significantly affects performance. We observe that when using the VORTEX consistency term on its own without any supervised or MC loss, it learns the trivial $f_\theta(\mathbf{y}, \mathbf{A}) = \mathbf{0}$, showing the superfluity of VORTEX on our experiments on in-domain data. Note that Noise2Recon [23] is a special case VORTEX with $\mathbf{T}_2 = \mathbf{I}$ and \mathbf{T}_1 is random noise.

Adversarial losses For the adversarial losses, we use the same model f_θ as the generator, and the simple convolutional discriminator with skip connections used in [17]. We perform generator and discriminator steps with ratio 1. Noting that there is a wide range of different GAN flavours, we use the MSE in the adversarial loss calculations following LSGAN [47].

MO-EI The MO-EI loss function is visualised diagrammatically in Fig. 4. We let $G = \text{Diffeo}(\mathbb{R}^2)$. As these are very general, we relax the full assumption and instead enforce approximate equivariance to small distortions by taking the subset of continuous piecewise-affine-based diffeomorphic transforms from [29, 84], visualised in Fig. 5. For MO-EI, we ablate the choice of transform in Appendix C.5.1.

Remark (MO-EI generalises MOI and EI). *By letting G be the trivial group, we recover MOI [78], and by letting $\mathcal{A} = \{\mathbf{A}\}$, we recover EI [12].*

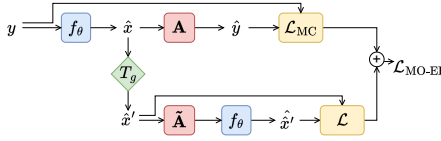


Figure 4: The multi-operator equivariant imaging (MO-EI) loss function.

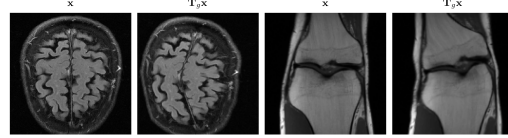


Figure 5: Diffeomorphic transforms.

B.3.1 Python implementations of benchmarked loss functions

Listing 1: Sketched pseudo-Python for our reimplementations of benchmarked loss functions $\mathcal{L}(\hat{\mathbf{x}}; \mathbf{y}, \mathbf{A}, f_\theta)$ in DeepInverse. See the benchmark site for how these are concretely called. Importantly, the GT \mathbf{x} is never used in loss calculation.

```
class MCLoss(Loss): # [70], Eq. (2)
    def forward(x_net, y, physics, model):
        return metric(physics.A(x_net), y)

class SplittingLoss(Loss): # [91], Eq. (3)
    def forward(x_net, y, physics, model):
        inp = Inpainting(mask = physics.mask - get_mask() * physics.mask())
        return metric((inp * physics).A(x_net), inp(y))

class ModelWrapper(Reconstructor): # Wraps f_theta
    # if eval_split_input = True, then this is [34], Eq. (4)
    def split(y, physics):
        inp = Inpainting(**mask_generator.step(physics.mask))
        return inp(y), inp * physics

    def forward(y, physics):
        if not eval_split_input and not training:
            return model(y, physics)
        else:
            x_net = sum(model(*split(y, physics)) for _ in range(N)) / N

class WeightedSplittingLoss(SplittingLoss): # [53], Eq. (5)
    P = physics_generator.step(1000).mean()
    P_t = mask_generator.step(1000).mean()
    K = (1 - P) / (1 - P_t * P)
    weight = (1 - K) ** -0.5
    metric = lambda y1, y2: metric(weight * y1, weight * y2)

class SplittingConsistencyLoss(SplittingLoss): # [35], Eq. (6)
    def forward(x_net, y, physics, model):
        x_net2 = model(y, physics)
        p2 = deepcopy(physics)
        p2.update(mask = 1 - physics.mask)
        return metric(p2.A(x_net), p2.A(x_net2)) + metric(y, physics.A(x_net)) + metric(y, physics.A(x_net2))

class MOILoss(Loss): # [78], Eq. (7)
    def next_physics(physics):
        p2 = deepcopy(physics)
        p2 = p2.update(**physics_generator.step())
        return p2
```

```

    def forward(x_net, y, physics, model):
        p2 = next_physics(physics)
        return metric(model(p2.A(x_net), p2), x_net)

class MOConsistencyLoss(MOILoss): # [95], Eq. (8)
    def forward(x_net, y, physics, model):
        metric_orig = metric
        metric = lambda a, b: a
        x2 = super().forward(x_net, physics, model)
        return metric_orig(y, physics.A(x2))

class EILoss(Loss): # [12], Eq. (9)
    def forward(x_net, y, physics, model):
        x2 = T(x_net)
        return metric(model(physics.A(x2), physics), x2)

class MOEILoss(EILoss, MOILoss): # M0-EI Loss Eq. (10)
    def forward(x_net, y, physics, model):
        return EILoss.forward(x_net, x, y, next_physics(physics), model)

class AugmentConsistencyLoss(Loss): # [22], Eq. (11)
    def forward(x_net, y, physics, model):
        x2 = T_2(physics.A_adjoint(T_1(y)))
        physics2 = physics * LinearPhysics( # Transform physics
            A=lambda x: T_2.inverse(x),
            A_adjoint=lambda x: T_2(x),
        )
        x3 = model(physics2.A(x2), physics2)
        return metric(T_2(x_net), x3)

class MultiOperatorUnsupAdversarialLoss(MOILoss): # [17], Eq. (12)
    def adversarial(real, fake):
        # Note m can be any GAN flavour e.g. LSGAN, WGAN [47]
        return m(D(fake), 1.) # for generator
        return m(D(real), 1.) + m(D(fake), 0.) # for discriminator

    def forward(x_net, y, physics, model):
        y_new = next_data()[1] # x, y
        physics_new = next_physics(physics)
        y_hat = physics_new.A(x_net)
        return adversarial( $F^H$ y_new,  $F^H$ y_hat) # iFFT

class UAIRGeneratorLoss(UnsupAdversarialLoss): # [61], Eq. (13)
    def forward(x_net, y, physics, model):
        physics_new = next_physics(physics)
        y_new = physics_new.A(x_net)
        return adversarial(y, y_new) + metric(y_new, physics_new.A(model(y_new, physics_new)))

class SUREGaussianLoss(Loss): # [76], Eq. (14)
    def div(*):
        y2 = physics.A(model(y + b *  $\tau$ , physics))
        return (b * (y2 - y_hat) /  $\tau$ ).mean()

    def forward(x_net, y, physics, model):
        y_hat = physics.A(x_net)
        b = randn(y.shape)
        return metric(y_hat, y) + 2 *  $\sigma^2$  * div(*) -  $\sigma^2$ 

class ENSURELoss(SUREGaussianLoss): # [5], Eq. (15)
    P = physics_generator.step(1000).mean()

    def metric(y_hat, y):
        return ( $F^H$ ((y_hat - y) / P.sqrt()) ** 2).mean() # from Eq. 12 of [5]

    def div(*):
        x2 = model(physics.A(physics.A_adjoint(y) + b *  $\tau$ ), physics)
        return (b * (x2 - x_net) /  $\tau$ ).mean()

class RobustSplittingLoss(WeightedSplittingLoss): # [54], Eq. (16)
    noise_model = GaussianNoise( $\sigma$  *  $\alpha$ )

    def forward(x_net, y, physics, model):
        loss = super().forward(x_net, y, physics, model)
        mask = get_mask() * physics.mask #  $M_{\lambda \cap \omega}$ 
        residual = mask * (physics.A(x_net) - y) * (1 + 1 / alpha ** 2)
        return loss + (residual ** 2).mean()

class ModelWrapper(SplittingLoss.ModelWrapper):

```



```

def split(y, physics):
    y, physics = super().split(y, physics)
    return mask * noise_model(y), physics

```

B.4 Python code for running benchmark using DeepInverse

The following Python code sketch can be used to train a reconstruction algorithm with the methods considered in this paper, where the loss functions loss can be replaced by those listed in Table 1. For full annotated training code, see the benchmark site.

Listing 2: Python script for training our benchmark experiments using DeepInverse.

```

import deepinv as dinv
import torch

# Define forward problem A
physics_generator = dinv.physics.generator.GaussianMaskGenerator((320, 320), acceleration=4)
physics = dinv.physics.MRI((320, 320))

# Define FastMRI dataset x
dataset = dinv.datasets.SimpleFastMRISliceDataset("data", train=True, download=True)
train_dataset, test_dataset = torch.utils.data.random_split(dataset, (0.8, 0.2))

# Simulate measurements (x,y)
dataset_path = dinv.datasets.generate_dataset(
    train_dataset=train_dataset,
    test_dataset=test_dataset,
    physics=physics,
    physics_generator=physics_generator,
    save_physics_generator_params=True,
    save_dir="data"
)

train_dataset = dinv.datasets.HDF5Dataset(dataset_path, split="train",
    load_physics_generator_params=True)
test_dataset = dinv.datasets.HDF5Dataset(dataset_path, split="test",
    load_physics_generator_params=True)

train_dataloader = torch.utils.data.DataLoader(train_dataset, shuffle=True)
test_dataloader = torch.utils.data.DataLoader(test_dataset)

# Define reconstruction  $f_\theta$ 
denoiser = dinv.models.UNet(2, 2, scales=3)
model = dinv.models.MoDL(denoiser=denoiser, num_iter=3)

# Define loss  $\mathcal{L}$  from those listed in Table 1
loss = ...

trainer = dinv.Trainer(
    model = model,
    physics = physics,
    optimizer = torch.optim.Adam(model.parameters(), lr=1e-3),
    train_dataloader = train_dataloader,
    eval_dataloader = test_dataloader,
    epochs = 100,
    losses = loss,
    metrics = dinv.metric.PSNR(complex_abs=True),
)

trainer.train()

```

C Further experimental results

C.1 Statistical significance results

To compare the performance of MO-EI with two next-best methods in scenario 1, we conduct two statistical tests: paired t -test (where normality of the differences is validated in Fig. 6), and Wilcoxon signed-rank. Results are shown in Table 6, suggesting, to a .1% significance level, that there is sufficient evidence to reject the null hypothesis and accept the alternative hypothesis that MO-EI has higher average performance.

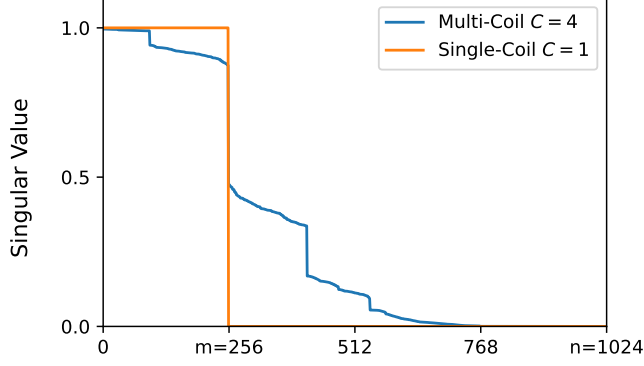


Figure 7: Numerical singular values of single-coil vs multi-coil operators, sorted in descending order.

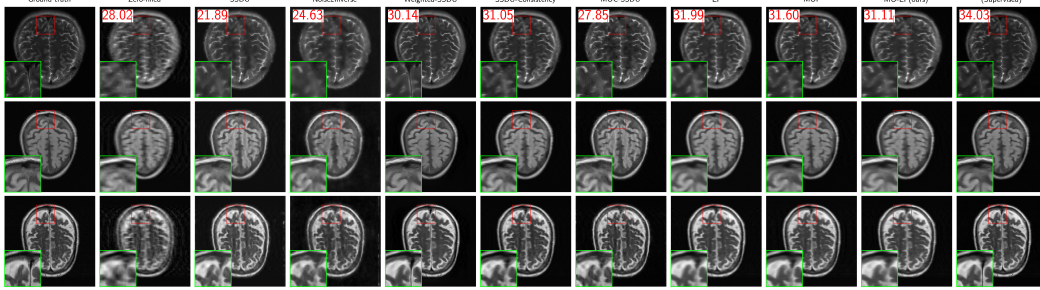


Figure 8: Sample reconstructions for scenario 3 (single-operator) with average test-set PSNR labelled. See Table 4 for full results.

Comparison	Paired t	Wilcoxon
MO-EI \leftrightarrow MOI	3.7×10^{-48}	6.0×10^{-17}
MO-EI \leftrightarrow SSDU-Consist.	6.4×10^{-44}	6.0×10^{-17}

Table 6: Statistical significance test p-values comparing test-set PSNR of top method (MO-EI) and the two next-best methods in scenario 1 (single-coil).

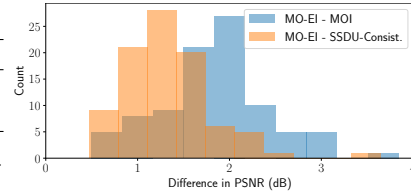


Figure 6: Histograms of paired diffs.

C.2 Rank of single-coil vs multi-coil operators

We further investigate the results of the multi-coil scenario by measuring the size of the null-space compared to the single-coil scenario. We consider a toy $4 \times$ accelerated MRI example on 32×32 images, so $n = 32 \times 32 = 1024$, $m = nC/4 = 256$ for single-coil and $C = 4$, $m = 1024$ for multi-coil. We then compute the numerical SVD of the operator \mathbf{A} ; results are in Fig. 7. The single-coil operator (scenario 1) has exactly $m = \text{rank}(\mathbf{A})$ non-zero singular values as expected, whereas the multi-coil operator (scenario 4) has many more non-zero singular values, increasing its effective rank [82] and decreasing the size of the “effective null-space”. For example, consider the case $\sigma = 0.1$; the effective $\text{rank}_{\sigma^2}(\mathbf{A}) = 686$, so the effective acceleration is $n/m = 1.49 < 4$. We hypothesise that this reduces the difficulty of learning in the null-space, and we leave for further work tuning the acceleration rate to achieve a similar effective rank as the single-coil case.

C.3 Scenarios 3 & 4

We provide sample reconstructions in Figs. 8 and 9 to complement the quantitative results given for Scenarios 3 (single-operator) & 4 (multi-coil) in Tables 4 and 5.

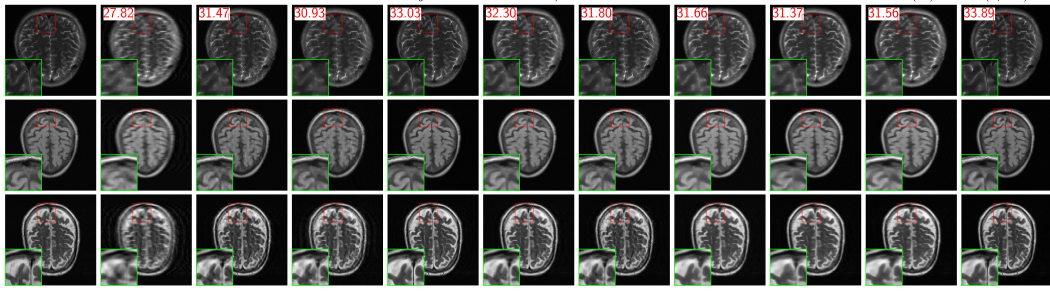


Figure 9: Sample reconstructions for scenario 4 (multi-coil) with average test-set PSNR labelled. See Table 5 for full results.

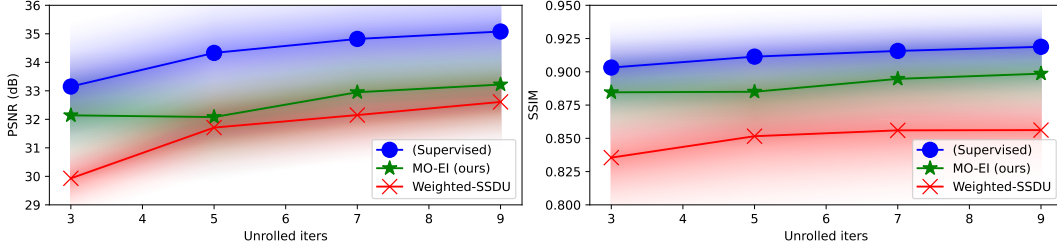


Figure 10: Quantitative results on scenario 1 for Weighted-SSDU, MO-EI, and oracle supervised losses for increasing number of unrolled iterations.

C.4 Unrolled depth

We investigate the effect of unrolling depth u (and hence time and memory cost) on performance scaling, starting at $u = 3$ (*i.e.* the model on which all results are reported in the main paper) up to $u = 9$. Results on scenario 1 are shown in Fig. 10 on two self-supervised losses and the supervised loss, showing a largely monotonic increase in performance as u increases, suggesting that results presented in the main paper would scale with more expensive models, and that there is a trade-off between model cost and performance.

C.5 Ablations

C.5.1 Ablation of MO-EI loss

We ablate for the components of our proposed loss function by interpolating between existing methods MOI and EI and the proposed method MO-EI, and report results in Table 7. We note that the base MOI and EI have similar results, and adding the two independent components of a) MO-EI and b) the diffeomorphic transforms helps, but combining these two provides the best performance in our proposed method, as per our theoretical framework.

C.5.2 Ablation of SSDU loss

We ablate for the components of SSDU [91] and weighted-SSDU [53] and report results in Table 8. While [91] construct variable-density 2D partitioning masks with an ACS block, we were only able to achieve good performance using uniform-density partitioning (*i.e.* Bernoulli) without an ACS block. We reproduce the weighted-SSDU results reported in [53]: results improve when adding the weighting even when using the original 2D partitioning, and improves further when using 1D partitioning masks, but only if these also do not have ACS lines.

C.6 Out-of-domain generalisation

Now suppose that GT data is available. We evaluate the robustness and generalisation of our models trained on brain data to out-of-domain, knee data. We compare a model trained with supervised learning on the brain data (scenario 1), our proposed self-supervised MO-EI method, and a model

Loss	PSNR \uparrow	SSIM \uparrow
MOI	30.29 \pm 2.88	.8651 \pm .0528
EI (rotate)	30.26 \pm 2.61	.8523 \pm .0542
EI (diffeo)	31.26 \pm 2.88	.8741 \pm .0522
MO-EI (rotate)	30.62 \pm 2.70	.8575 \pm .0553
MO-EI (diffeo, ours)	32.14\pm2.73	.8846\pm.0498

Table 7: Ablation of components of the proposed MO-EI loss function.

Loss	PSNR \uparrow	SSIM \uparrow
SSDU (uniform-density no ACS)*	27.98 \pm 1.43	.7485 \pm .0667
SSDU (variable-density with ACS)	18.27 \pm 1.01	.4876 \pm .0598
Weighted-SSDU (1D partition)*	29.93\pm1.66	.8355\pm.0626
Weighted-SSDU (2D partition)	28.62 \pm 1.59	.7489 \pm .0692
Weighted-SSDU (1D with ACS)	13.41 \pm .63	.3875 \pm .0479
SSDU (1D partition)	27.38 \pm 1.87	.8055 \pm .0658

Table 8: Ablation of components of SSDU [91] and weighted-SSDU [53] loss functions. * = methods reported in main paper.

trained alternating between supervised and self-supervised (“interleaved”) losses. The results in Table 9 show that, even when GT is available, adding a self-supervised loss during supervised training highly improves the robustness of the model. Qualitatively, the pure supervised model places strange brain-like artifacts in the knees in Fig. 11, where the interleaved training removes this while retaining a sharp image.

C.7 Transfer of benchmark to different imaging modality

We demonstrate the transferability of our modular benchmark on a different scientific imaging modality where GT images do not exist. Hyperspectral imaging aims to obtain high quality multi-channel images of the Earth for remote sensing and environmental monitoring, but observations may be degraded due to impulse noise arising from missing lines and thermal noise [62, 8, 74]. Hyperspectral restoration is therefore an important preprocessing task, but GT is unavailable [8, 74] because of the non-stationary nature of satellites.

Our modular benchmark framework facilitates evaluating SSI methods on any imaging inverse problem such as the hyperspectral restoration problem, and we demonstrate a proof-of-concept showing the ease of adapting the benchmark to a different problem domain. Concretely, we simply swap out the following modules:

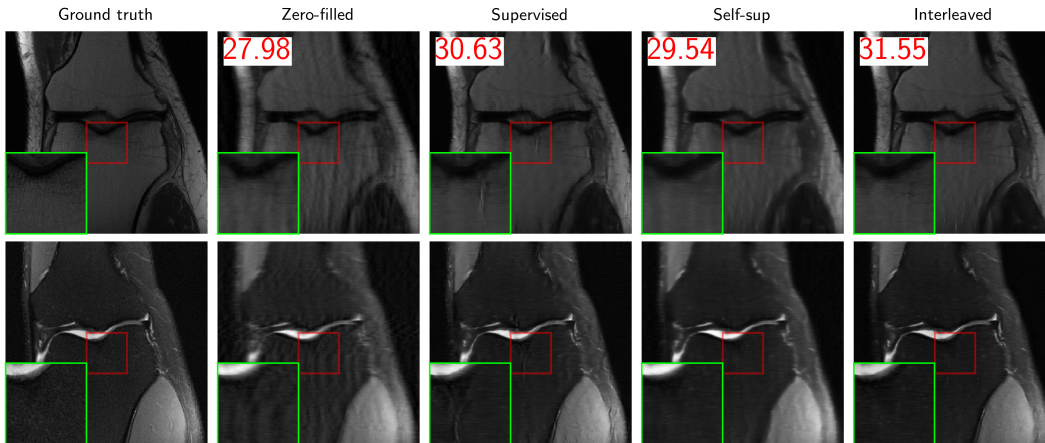


Figure 11: Sample reconstructions for out-of-domain generalisation experiments trained on $6\times$ acc. brains and tested on $6\times$ acc. knees with average test-set PSNR labelled.

Loss	PSNR \uparrow	SSIM \uparrow
Supervised	30.63 \pm 1.89	.7759 \pm .0676
Self-supervised	29.54 \pm 1.83	.7390 \pm .0721
Interleaved	31.55\pm1.98	.7910\pm.0682

Table 9: Out-of-domain generalisation results for $6\times$ accelerated MRI trained on the FastMRI brain dataset and tested on knees.

Loss	PSNR \uparrow	SSIM \uparrow
Zero-filled	15.53 \pm .59	.1435 \pm .01
ENSURE	16.69 \pm .75	.2074 \pm .0155
Robust-SSDU	24.05 \pm .31	.4965 \pm .0236
Noise2Recon-SSDU	23.87 \pm .75	.5216 \pm .0366
Robust-EI	25.72\pm.72	.6601\pm.0243
Robust-MO-EI	25.64 \pm .72	.6535 \pm .0242
(Supervised)	26.69 \pm .70	.7282 \pm .0201

Table 10: Test-set results for hyperspectral image restoration.

1. `physics = deepinv.physics.MRI() \rightarrow deepinv.physics.Inpainting(noise_model=deepinv.physics.GaussianNoise())`, *i.e.* random inpainting with 1D masks (50% dropout) with additive noise ($\sigma = 0.1$);
2. `dataset = FastMRISliceDataset(...) \rightarrow NBUDataset(...)`, where we use a subset of $150\ 256 \times 256 \times 4$ WorldView-2 satellite patches provided by [51].

Qualitative and quantitative results are shown in Fig. 12 and Table 10, benchmarking self-supervised losses for joint reconstruction and denoising, with the no-learning result showing the input since $\mathbf{A}^\top \mathbf{y} = \mathbf{y}$. The results show the superiority of Robust-EI, with ENSURE failing to recover information in the null-space, and Robust-SSDU and Noise2Recon-SSDU less able to produce spatially and spectrally faithful reconstructions. We hypothesise that Robust-MO-EI performs less well due to the inappropriate application of diffeomorphic invariance to urban satellite images, where straight lines should remain straight.

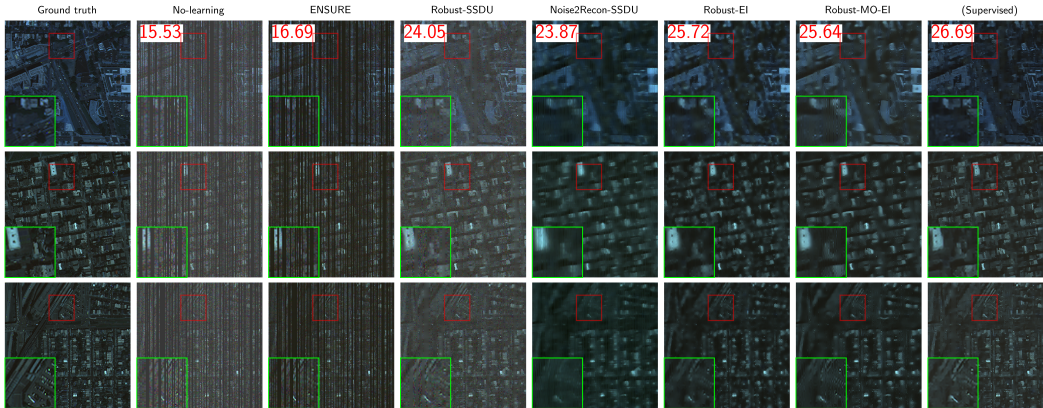


Figure 12: Sample reconstructions for hyperspectral image restoration.